Apigenin C-Glycosides of *Microcos paniculata* protects lipopolysaccharide induced apoptosis and inflammation in acute lung injury through TLR4 signaling pathway

Kunping Li[1,7†], Zhuoru He[1,7†], Xinqiuyue Wang[2†], Miguel Pineda[3], Runbao Chen[4], Haiqi Liu[2], Kaiting Ma[2], Huanjia Shen[2], Chunhui Wu[4], Ningtin Huang[5], Tianling Pan[1,7],Yun Liu[6*], Jiao Guo[7*]

[1]School of Pharmacy, Guangdong Pharmaceutical University, Guangzhou 510006, China,
[2]School of Pharmaceutical Sciences, Guangzhou Medical University, Guangzhou 511436, China,
[3]Institute of infection, immunity & inflammation, University of Glasgow, University Place, Glasgow G12 8TA, UK,
[4]the Second Clinical School, Guangzhou Medical University, Guangzhou 511436, China,
[5]School of Agriculture and Biology, Shanghai Jiao Tong University, Shanghai 200240, China,
[6]Key Laboratory of Molecular Target & Clinical Pharmacology, School of Pharmaceutical Sciences & the Fifth Affiliated Hospital, Guangzhou Medical University, Guangzhou 511436, China
[7]Institute of Chinese Medicinal Sciences, Guangdong Pharmaceutical University, Guangzhou 510006, China

[†]These authors contribute equally to this work.

Running title: ACGs of *M. paniculata* exerts anti-apoptotic and anti-inflammatory activities

[*]Correspondence:

Dr. Yun Liu

Address: Key Laboratory of Molecular Target & Clinical Pharmacology, School of Pharmaceutical Sciences & the Fifth Affiliated Hospital, Guangzhou 511436, China

Tel: + 86-20-37103630 Fax:+86-20-37103630; E-mail: liuyun195@sina.com

Prof. Dr. Jiao Guo

Institute of Chinese Medicinal Sciences, Guangdong Pharmaceutical University

280 East Road, Outer Ring, Guangzhou Higher Education Mega Center, Guangzhou 510006, China

Tel: + 86-20-39352818; Fax: +86-20-39352818; E-mail: gyguoyz@163.com

Abstract

Acute lung injury (ALI) and its more severe form acute respiratory distress syndrome (ARDS) are life-threatening conditions with high morbility and mortality, underscoring the urgent need for novel treatments. Leaves of the medicinal herb *Microcos paniculata* have been traditionally used for treating upper airway infections, by virtue of its content of flavonoids such as apigenin C-glycosides (ACGs). C-glycosides have been shown to exert strong anti-inflammatory properties, although their mechanism of action remains unknown. Herein, hypothesizing that ACGs from *M. paniculata* inhibit progression of ALI, we used the experimental model of lipopolysaccharide (LPS)-induced ALI in BALB/c mice to evaluate the therapeutic potential of purified ACGs. Our results showed that *M. paniculata* ACGs inhibited lung inflammation in animals undergoing ALI. The protective effects of ACGs were assessed by determination of cytokine levels and in situ analysis of lung inflammation. ACGs reduced the pulmonary edema and microvascular permeability, demonstrating a dose-dependent down-regulation of LPS-induced TNF-α, IL-6 and IL-1β expression in lung tissue and bronchoalveolar lavage fluid, along with reduced apoptosis. Moreover, metabolic profiling of mice serum and subsequent Ingenuity Pathway Analysis suggested that ACGs activated protective protein networks and pathways involving inflammatory regulators and apoptosis-related factors, such as JNK, ERK1/2 and caspase-3/7, suggesting that ACGs-dependent effects were related to MAPKs and mitochondrial apoptosis pathways. These results were further supported by evaluation of protein expression, showing that ACGs blocked LPS-activated phosphorylation of p38, ERK1/2 and JNK on the MAPKs signaling, and significantly upregulated the expression of Bcl-2 whilst down-regulated Bax and cleaved caspase-3. Remarkably, ACGs inhibited the LPS-dependent TLR4 and TRPC6 upregulation observed during ALI. Our study shows for the first time that ACGs inhibit acute inflammation and apoptosis by suppressing activation of TLR4/TRPC6 signaling pathway in a murine model of ALI. Our findings provide new evidence for better understanding the anti-inflammatory effects of ACGs. In this regard, ACGs could be exploited in the development of novel therapeutics for ALI and ARDS.

Key Words

Microcos paniculata, apigenin C-glycosides, acute lung injury, metabolic profiling, GC-MS, MAPKs, TLR4, TRPC6, Ingenuity Pathway Analysis.

INTRODUCTION

Acute lung injury (ALI) and its more severe form, acute respiratory distress syndrome (ARDS), are life-threatening medical conditions triggered by common pathologies such as trauma, pneumonia or sepsis. As a consequence, patients develop hypoxemic respiratory failure with high morbidity and mortality rate. ALI pathophysiology is characterized by increased permeability of the alveolar-capillary barrier and pulmonary edema as a result of macrophage activation and extensive neutrophil influx into the lungs. Infiltrating cells release cytokines that activate local pro-inflammatory networks, leading to irreversible damage of the lung epithelium and endothelial cells (1,2).

Lipopolysaccharide (LPS), a main component of the out membrane of gram-negative bacteria, has been identified as a potent inducer of bacterial sepsis-induced ALI (3,4,5). Upon stimulation by LPS, Toll-like receptor 4 (TLR4) expressed in macrophages and endothelial cells is recruited to lipid rafts and interacts with different adaptor molecules (6,7), resulting in activation of downstream signaling pathways responsible for the production of pro-inflammatory cytokines and subsequent infiltration of inflammatory cells, such as neutrophils, into the lungs (8). This uncontrolled inflammatory responses finally induce loss of normal alveolar capillary barrier function and pulmonary edema (6,7). In this regard, transient receptor potential channel 6 (TRPC6), a permeable non-selective cation channel, has been shown to modulate Ca^{2+} entry into endothelial cells to further enhance TLR4-dependent vascular permeability and local inflammation in the lung (9,10). Thus, targeting the TLR4/TRPC6 axis in endothelial cells might offer novel therapeutic targets to inhibit aberrant pro-inflammatory cytokine networks in the lungs of ALI patients. However, despite our increasing understanding of the pathophysiology of ALI and ARDS (11,12), there is still an alarming lack of therapeutic agents to treat these conditions and the mortality rate remains high, reflecting that key events regulating pathogenesis remain elusive. Indeed, the only effective therapy against ALI consists of mechanical ventilation and there is no pharmacological approach available (13). Thus, developing novel therapeutics for ALI is an urgent and unmet clinical need.

Microcos paniculata, also known as shiral (India, Bengal), is an edible and medicinal plant, whose leaves (*Microctis folium*) have been used in traditional medicine for hundreds of years to relieve diseases and infections affecting the upper respiratory tract involving fever, throat irritation, cough or phlegm (14). It has been proved that *M. paniculata* total flavonoids are responsible for its main

therapeutic effects, which is coincided with its anti-oxidative and anti-inflammatory abilities (15). However, little is known about the bioactivity of the apigenin C-glycosides (ACGs), the main sub-fraction found in *M. paniculata* total flavonoids. Recent work suggests that ACGs may act as strong anti-inflammatory compounds (16,17,18,19), although the molecular mechanism of the anti-inflammatory actions elicited by ACGs is still unknown.

In this study, we isolated and characterized *M. paniculata* ACGs fraction to test its anti-inflammatory potential in the LPS-induced model of ALI in Balb/c mice. Our results show that ACGs are effective at inhibiting disease progression and this was associated with a clear reduction in cellular infiltration and local inflammation as shown by histological analysis and cytokine production, such as IL-6, IL-1β and TNF-α. This provides proof of concept in the *in vivo* model that such compounds can be active against ALI. Furthermore, we elucidated the underlying mechanism using metabolomics analysis combined with Ingenuity Pathway Analysis, IPA. Metabolomics, which focus on a comprehensive analysis of small molecule metabolites (< 1 kDa), is highly propitious to the discovery of novel biomarkers and therapeutic targets in biomedicine (20,21). Combined with IPA, metabolomics is acting as one cutting-edge tool for pharmacological research (22,23,24), especially for illustrating the molecular mechanism of bioactive natural products. This approach revealed that ACGs inhibited the MAPKs pathway and apoptosis pathway. Moreover, we also identified the TLR4/TRPC6 axis as a critical pathway down-regulated by ACGs to mediate protection in ALI mice.

Collectively, our data contribute to the identification of the TLR4/MAPKs/TRPC6 axis as therapeutic target in ALI and suggest that ACGs extracted from *M. paniculata* could offer new molecules to therapeutically intervene these inflammatory and apoptosis pathways.

RESULTS

Preparation, qualitative and quantitative profiling of ACGs fraction from M. paniculata

To separate the ACGs from *M. paniculata* in one fraction, 5 kg of *M. paniculata* leaves were used to isolate 7.9 g of ACGs spray-dried powder through systematic purification as described in material and methods. Liquid Chromatography Quadrupole Time-of-Flight Mass Spectrometry (LC-qTOF-MS) was conducted on the isolated product to further identify the main components present in the ACGs fraction. Using the retention time, accurate molecular weight and the MS/MS fragmentation

pattern with standards, eight apigenin C-glycosides were unequivocally identified, namely, vicenin-2, isoshaftoside, shaftoside, vitexin, vicenin-1, isovitexin, violanthin, isoviolanthin. (Fig. 1A-H). These 8 molecules represented around 75% of the total content of ACGs, as shown by quantitative HPLC analysis (Fig. 1I-J).

ACGs exert protective effects against LPS-mediated ALI in vivo

LPS-induced ALI, a well-characterized model of the human ALI (25), was employed for testing the therapeutic potential of the isolated ACGs fraction from *M. paniculata* leaves. To investigate the therapeutic effects of ACGs, mice undergoing ALI were treated with ACGs (10, 20, 40 mg/kg) and lung tissues were removed after dissection and stained with hematoxylin and eosin (H&E). As expected, LPS challenge induced distinct histological changes compared to tissue from naïve animals, including interstitial edema, alveolar wall thickening and a mass of inflammatory cells infiltrating into the lung alveolar spaces (Fig. 2). However, ACGs treatment significantly alleviated these LPS-induced pathological changes in a dose-dependent manner (Fig. 2). Remarkably, ALI mice treated with 40 mg/kg of ACGs displayed a lung architecture similar to naïve animals or mice treated with dexamethasone (Fig. 2). To assess whether ACGs had anti-inflammatory actions per se, or they were simply preventing LPS binding to TLR4 and/or its subsequent activation, the flavonoids were administered to mice that had received LPS injections 24h before. Remarkably, ACGs still reduced lung inflammation significantly (Fig. S1), demonstrating an intrinsic anti-inflammatory activity.

To further evaluate the protective effects of ACGs during experimental ALI, several parameters related to LPS-induced pulmonary edema and microvascular permeability were quantified, such as wet/dry lung weight ratio, neutrophil infiltration, protein concentration in bronchoalveolar lavage fluid (BALF) and myeloperoxidase (MPO) activity in lung tissue (Fig. 3). Treatment with ACGs (as in Fig. 1) essentially abrogated LPS-induced pulmonary edema and microvascular permeability, as evidenced by a significant reduction of i) lung wet/dry weight ratio (Fig 3A), ii) number of neutrophils and iii) protein content in BALF (Fig. 3B,C) and iv) MPO activity in tissue extracts (Fig. 3D). Interestingly, ACGs at 40 mg/kg exerted again an anti-inflammatory effect similar, or even better, than dexamethasone. Similar results were observed when ACGs treatment was given 24h post LPS treatment (Fig. S2). These results indicate that ACGs induce a strong protective effect on the alveolar-

vascular barrier integrity, inhibiting influx of inflammatory cells, lung edema and cellular damage triggered by LPS.

ACGs inhibit cytokine secretion and apoptosis in LPS-induced ALI

As local expression of pro-inflammatory TNF-α, IL-6 and IL-1β has been shown to be critical for infiltration of neutrophils in the lungs during ALI progression, we also investigated whether ACGs down-regulated the expression of these cytokines *in vivo*. Therefore, relative mRNA expression for TNF-α, IL-6 and IL-1β was evaluated in lung tissue by quantitative PCR (Fig. 4A-C) and protein levels were quantified in BALF by ELISA (Fig. 4D-F). Results showed that ACGs inhibited the LPS-mediated up-regulation of TNF-α, IL-6 and IL-1β observed in mice undergoing ALI. Likewise, ACGs inhibited cytokine production in a dose-dependent manner, similarly to the protective effects associated to ACGs treatment in ALI mice in the histopathological and microvascular permeability analysis (Fig. 2&3) . Likewise, ACGs treatment 24h post LPS injection significantly reduced TNF-α and IL-6 in BALF in a dose-dependent manner (Fig. S3). Moreover, confirming the anti-inflammatory activity of ACGs, the flavonoids strongly inhibited LPS-mediated macrophage cytokine production *in vitro* (Fig. S4).

Finally, we examined the epithelial and endothelial cell apoptosis, since it has been shown that increased apoptosis reflects the degree of tissue damage in lungs from ALI patients (26,27). To determine whether ACGs diminished apoptosis (and subsequent tissue damage) in ALI mice, we employed TUNEL staining to quantify the number of apoptotic cells in lung tissues (Fig. 4). As expected, LPS-treated group showed a significant increase of apoptotic cells compared to the PBS-treated control group. However, treatment with ACGs led to significant and dose-dependent reduction in the number of apoptotic cells (Fig. 4G-H). These findings indicate that ACGs treatment inhibited apoptosis in the lungs of ALI mice.

Serum metabolic profiling showed distinct metabolite composition in response to ACGs.

Collectively, our data provide compelling evidence for a protective effect of ACGs in the experimental LPS-dependent ALI-model. However, the molecular mechanisms triggered by ACGs were still unknown. Arachidonic acid and other polyunsaturated fatty acids are precursors of prostaglandins, leukotrienes and related compounds that have important roles as inflammatory

mediators. As it is known that some flavonoids inhibit fatty acid-induced signaling by suppressing TLR4 function, we hypothesized that ACGs rewired lipid metabolism to inhibit LPS signaling and subsequent TLR4-dependent inflammation. Thus, we conducted targeted fatty acids profiling and non-targeted metabolic profiling on gas chromatography mass spectrometry (GC-MS, typical total ion chromatograms are shown in Fig. S6). We used principal component analysis (PCA) for multivariate analysis of the targeted fatty acids profiling data and non-targeted metabolic profiling data of control group, LPS group and ACGs (40 mg/kg) group. Data analysis identified a clear metabolic pattern associated to both LPS activation and ACGs treatment (Fig. 5).

Likewise, data were subjected to significant difference analysis on SPSS and partial least square discriminant analysis (PLS-DA)/orthogonal partial least square discriminant analysis (OPLS-DA) on Simca-p to figure out the p-values and VIP values respectively (Fig. S7). Significant differences between LPS group and ACGs group (40 mg/kg) were filtered by establishing $p < 0.05$ and $VIP > 1$ as the threshold. As a result, 30 metabolites, including palmitic acid (C16:0), stearic acid (C18:0), linoleic acid (C18:2n6c), arachidonic acid (C20:4n6), glyoxylic acid, 3-hydroxybutyric acid and taurine, were found to be differentially expressed (Table 1). This allowed us to define a metabolomics signature of ACGs biological actions.

Ingenuity Pathway Analysis of metabolomics data suggested that ACGs targets MAPKs pathway and mitochondrial apoptosis in vivo to exert their anti-inflammatory activity.

To further address the mechanisms underlying ACGs-mediated protection in ALI, differentially expressed metabolite profiling data were further analyzed using Ingenuity Pathway Analysis (IPA) software to interpret the biological changes, altered canonical pathways and gene networks. IPA exploits relationships among differential metabolites or genes expression and it is a powerful tool for identification of significantly changed pathways in drug discovery. Therefore, we next decided to perform IPA analysis on the metabolites regulated by ACGs (Table 1), with the goal of constructing the molecular interaction networks underlying the molecular mechanism of *M. paniculata* ACGs fraction on treating ALI. The highest-scoring (IPA score, 43) network targeted by ACGs involved 16 molecules (Fig. 6) and highlighted two major pathways (Table S1). Interestingly, this network involved inflammatory regulators and apoptosis-related factors directly related to modulation of the generic mitogen-activated protein kinases (MAPKs) pathway and mitochondrial apoptosis pathway,

such as c-Jun N-terminal kinase (JNK), extracellular regulating kinase 1/2 (ERK 1/2) and caspase-3/7. This indicated that the anti-inflammatory mechanism of ACGs might involve down-regulation of MAPKs-dependent pathways, as well as mitochondrial apoptotic pathways.

ACGs targeted MAPKs to down-regulate inflammatory responses, whilst inhibition of apoptosis relied on modulation of mitochondrial-dependent pathways.

Since MAPKs are reported to be activated in LPS-induced inflammatory process, we decided to evaluate activation of the MAPKs pathway in the lung tissue of ALI mice treated with ACGs *in vivo* compared to control mice. Confirming the results generated by IPA analysis, ACGs efficiently blocked LPS-dependent phosphorylation of p38, ERK1/2 and JNK (Fig. 7A-D), as evaluated by western blotting. Similarly, we also measured expression of described mitochondrial apoptosis-related factors, both anti-apoptotic, Bcl-2, and pro-apoptotic, Bax and caspase-3. Whilst LPS down-regulated the expression of Bcl-2, ACGs treatment restored the expression of Bcl-2 to homeostatic levels (Fig. 7E, F), suggesting that ACGs maintained Bcl-2 activity to inhibit apoptosis. Moreover, compared with the control group, LPS induced a marked increase in the expression of anti-apoptotic Bax and cleaved caspase-3, which were attenuated by ACGs treatment (Fig. 7E, G, H). On the basis of these results, we concluded that ACGs suppressed apoptosis in LPS-induced ALI by targeting apoptotic through mitochondrial pathways.

TLR4 activation of TRPC6 signaling pathway is involved in LPS-induced ALI

Given the strong down-regulation of MAPKs activation by ACGs (which was even more powerful than dexamethasone when used at 40 mg/kg), we hypothesized that additional mechanisms may be triggered by ACGs to deactivate LPS-mediated TLR4 signaling. Regarding this, it has been described that Ca^{2+} entry upon activation of TRPC channels accounts for the increased permeability and inflammation of lung. Therefore, we hypothesized that TLR4 interferes with TRPC channels function in mediating lung vascular leakage and inflammation. To test this hypothesis, we examined the expression of TLR4 and TRPC6 in mice undergoing ALI in the presence or absence of increasing concentrations of ACGs as before. Interestingly, we observed that ACGs down-regulated expression of both TLR4 and TRPC6 induced by LPS *in vivo* (Fig. 8A-C).

DISCUSSION

In the present study, we have set up a simple process to isolate ACGs from *M. paniculata* leaves and we found that ACGs attenuated LPS-induced ALI through modulation of TLR4/TRPC6 pathway, reducing the release of pro-inflammatory cytokines, and regulating the expression of apoptosis-related factors. Thus, our results show that ACGs contain valuable therapeutic potential for human ALI.

We chose the LPS-induced ALI to test the therapeutic potential of ACGs because it is a well-accepted model of human ALI, since it recapitulates important aspects of the human disease, such as the disrupted alveolar epithelial and endothelial barrier function, cell infiltration, and local inflammatory responses (25,28). Given the success of *M. paniculata* in traditional medicine to treat pulmonary inflammation, it was important to isolate and characterize its bioactive molecules. Even though previous studies in the last 20 years suggested that some anti-inflammatory substances (glucocorticoids, inhaled nitric oxide or Ketoconazole) (29,30) exert anti-inflammatory responses during LPS-induced ALI, none of these drugs has been translated to therapy, and are limited to assist in disease management. Thus, there is still an urgent need for pharmacological options, that could be found in *M. paniculata* ACGs. We demonstrated that ACGs protect against LPS-induced ALI by exerting a number of synergistic actions *in vivo*, including inhibition of interstitial edema, maintenance of alveolar–capillary barrier and reduction of cytokine production and infiltration of activated neutrophils. Neutrophils are key disease mediators in the lungs, since they induce tissue damage by releasing pro-inflammatory cytokines and generating reactive oxygen species (ROS) (31,32). Accordingly, depletion of neutrophils inhibited progression of experimental ALI and neutrophils in the BALF of patients with ARDS is associated with a poor disease outcome (33). Interestingly, we observed that ACGs-mediated protection during ALI was associated with, not only a reduction of neutrophil infiltration in the lungs, but also a reduced cell activation. This is the first observation of an anti-inflammatory molecule inhibiting neutrophil-dependent inflammatory responses in ALI. Supporting this, ACGs treatment down regulated expression of pro-inflammatory cytokines such as TNF-α, IL-6 and IL-1ß, both in the lung tissue and BALF. Therefore, our results provide evidence for a novel anti-inflammatory role of ACGs at multiple levels, including neutrophil recruitment and activation, pro-inflammatory cytokine networks and epithelial barrier permeability. ACGs also reduced LPS-mediated inflammation 24h after the challenge, demonstrating that ACGs might have

anti-inflammatory activity directly (via a mechanism that might be independent of competing for TLR4 binding) such as inhibition of caspases and Bcl-2 family members, well-known regulators of apoptosis, or the observed regulation of the three apoptosis-related molecules targeted by ACGs *in vivo*: Bcl-2, caspase-3 and Bax. In line with this, many studies have shown that increased apoptosis of epithelial and endothelial cells significantly contribute to compromise the alveolar-capillary barrier integrity (34). Nevertheless, direct and indirect mechanisms to suppress TLR4 activation are not mutually exclusive and both might be acting synergistically upon ACGs treatment.

To further explore the mechanisms underlying the ACGs actions, we evaluated fatty acid metabolism, as hydrophobic fatty acids are precursors of prostaglandins and leukotrienes, crucial inflammatory molecules that provide a link between cellular metabolism and inflammation, which could explain the diverse anti-inflammatory mechanisms triggered by ACGs *in vivo*. In fact, some flavonoids have been shown to inhibit fatty acid-induced signaling by uncoupling TLR4-dependent pathways. Although it is still not completely understood how ACGs-dependent modulation of metabolite networks can regulate inflammatory responses, it is becoming increasingly clear that metabolism and inflammatory mechanisms are intimately connected. For example, the most elevated metabolites in ACGs-treated mice are β-hydroxybutyrate, L-asparagine and taurine, that have been reported to inhibit NLRP3 inflammasome (35), AMP-activated protein kinase signalling pathways (36) and IL-1β and IL-6 expression (37,38) respectively, suggesting that ACGs rewire cellular metabolism towards a less inflammatory phenotype to control progression of ALI.

Using the bioinformatic IPA integrated with the current understanding of signaling pathways, analysis of the full list of modulated metabolites allowed us to generate a molecular network to reveal that ACGs targeted MAPKs pathway and mitochondrial apoptosis pathways, both major regulators of inflammation. Indeed, some of the ACGs described here, such as vitexin and isovitexin, have been defined as inhibitors of MAPKs pathways in other inflammatory conditions (39,40). Confirming this, our data show that ACGs have a strong potential to specifically inhibit MAPK-dependent inflammation, as they reduced ERK1/2, JNK and p38 activation upon LPS challenge. However, MAPKs are known to modulate many inflammatory mediators, suggesting that ACGs may affect production of other mediators not identified in this study. Similarly, it is known that LPS-dependent activation of TLR4 is involved in neutrophil activation and recruitment to the lungs during ALI, and

TLR4 activation in endothelial and epithelial cells also contributes to the loss of lung vascular barrier function(10,32,33). In relation with this, elevated levels of intracellular Ca^{2+} seem to precede endothelial and epithelial cells barrier dysfunction (41), but it is unknown whether Ca^{2+} signaling pathways intersect with TLR4 signalling in ALI, or whether these contribute to LPS-induced inflammation and apoptosis. We observed that ACGs inhibited the expression of TLR4, which could explain some of the anti-inflammatory actions described before, like the reduced IL-1β , IL-6 and TNF-α expression, or the inhibition of the MAPKs pathway, but rather interestingly, ACGs also down-regulated expression of TRPC6, a member of the Ca^{2+} permeable Transient Receptor Potential (TRP) channels (42,43), perhaps providing in ALI a synergistic mechanism between intracellular Ca^{2+} influx and TLR4/mediated inflammation as proposed before (44). ACGs might inhibit the increase of intracellular Ca^{2+} upon TLR4/TRPC6 activation and associated MAPKs pro-inflammatory signaling, which results in increased pro-inflammatory cytokine production and apoptosis of endothelial cells and subsequent loss of endothelial barrier integrity.

Thus, although full understanding of the mechanisms underpinning ACGs-mediated protection in ALI requires further work, we propose that ACGs target the TLR4/TRPC6 inflammatory system, activated upon LPS interaction during ALI initiation. By targeting this inflammatory cascades, ACGs may protect against ALI in a novel and highly efficient way (Fig. 9). Therefore, this study indicates that there is great medicinal potential to be found amongst the ACGs isolated from *Microcos paniculata*. Furthermore, *M. paniculata* has been used for centuries in China as medicinal herb, and it is currently employed in commercialized herbal tea in China, suggesting that anti-inflammatory compounds based on *M. paniculata* ACGs might not have significant drawbacks or immunosuppressive side-effects often associated to other anti-inflammatory therapies. Thus, the structures elucidated here might provide a novel platform for a rational development of novel and safer anti-inflammatory drugs to treat human ALI, but perhaps to other inflammatory conditions, where TLR4-dependent signaling plays a crucial role in disease initiation and progression as well.

MATERIALS AND METHODS

Preparation of M. paniculata ACGs fraction

Dried *M. paniculata* leaves (5 kg) were extracted with water (80 L, 2 times) at 95~100 °C for 2 h. The water filtrate was concentrated and passed through a D101 macro-porous resin column (i.d. 20

cm × 150 cm, Xi'an Sunresin New Materials Co. Ltd., China) and then eluted with 10%, 70% and 95% EtOH. The 70% EtOH eluate was further purified with Sephadex LH-20 column (GE healthcare, 7 cm × 60 cm) with MeOH-H_2O (80:20), and the purified flavonoids were further separated by preparative HPLC with C18 column (20 mm × 250 mm, 10 μm, Hanbang technology Co., Ltd, China) and the elution rich of ACGs was then collected, concentrated and spray-dried.

The specific compounds of ACGs were further isolated and purified using semi-preparative high performance liquid chromatography, and then characterized using ^{1}H-NMR, ^{13}C-NMR and HRMS.

Ultra performance liquid chromatography time of flight mass spectrometry analysis

Identification of compounds from *M. paniculata* ACGs fraction was carried out using a 1290 UHPLC-6545-QTOF-MS (Agilent Corporation, MA, USA) (45). The mobile phase was a mixture of methanol (A) and water containing 0.05% formic acid (B) using a liner gradient of 0-7.6 min，85% → 60% (B)；7.6-10 min, 60% → 60% (B)；10-12 min, 60% → 30% (B)；12-15 min, 30% → 20% (B)；15-16 min, 20% → 0% (B)；16-20 min, 0% → 0% (B). The flow rate was set as 0.2 mL/min and injection amount was 2 μL. The column temperature was set to 35 ℃. Mass spectrometry was programmed in a negative ion mode with a scan scale of 50-1000 m/z. The source temperature was set to 150 ℃ and a source voltage was 3.5 kV. The wavelength for ultraviolet (UV) detector was 276 nm.

High performance liquid chromatography analysis

Quantitative profiling of *M. paniculata* ACGs fraction was performed on HPLC (LC-20AT, Shimadzu, Japan) with a Kromasil C18 column (250 mm×4.6 mm, 5 μm) (46). The mobile phase was methanol (A) and water containing 0.2% phosphoric acid (B) with a flow rate of 1 mL/min, using a gradient of 0-12 min, 82% → 70% (B); 12-45 min, 70% → 55% (B); 45-60 min, 55% → 20% (B). The injection volume was 10 μL and the wavelength for UV detector was 276 nm.

Animals and LPS-induced ALI

Male Balb/C mice were obtained from Guangzhou University of Chinese Medicine (Guangzhou, China). Animal study protocols were reviewed and approved by the Ethics Committee of Guangzhou Medical University. All animals studies were conducted in accordance with the ARRIVE (Animal Research: Reporting of *In Vivo* Experiments) guidelines for reporting experiments involving animals (47,48). Mice, 8-10 weeks, were randomly divided into the following six groups (n=12): control, LPS,

LPS+ACGs (10 mg/kg, 20 mg/kg and 40 mg/kg), LPS+Dexamethasone (Dex, 10 mg/kg). ALI was induced by intratracheal instillation of LPS (Sigma, *E.coli 055:B5*, 2 mg/kg, dissolved in PBS) according to previous study with minor modifications (49). Mice treated with PBS in a similar way was used as a non-inflammatory control. ACGs was given for three times by intragastric administration (an equal volume of 0.5% CMC-Na (carboxymethycellulose sodium) was given to control group) and Dex was administered three times by intraperitoneal injection in LPS-treated group mice at days -1, 0 and +1, being day 0 the day of the LPS administration. For day 0, both ACGs and Dex were injected 2 hours prior to the LPS challenge. 48 hours after LPS administration, lung tissues, serum and BALF were harvested. All animals were maintained under standard laboratory conditions, housed with 12 h light/dark cycles at controlled 22-24 °C and 60-65% humidity. A total of 90 mice were used in this study, and the mice were acclimatized to the environment for 7 days before experiments.

Histopathologic evaluation of the lung tissue

Lung tissues were washed three times with cold PBS and fixed in 4% paraformaldehyde followed by paraffin embedding, then cut into 4 μm sections, and stained with hematoxylin and eosin (H&E). Pathological changes in the lung tissues were evaluated by light microscope.

Lung wet/dry ratio

The middle lobe of right lungs were harvested and weighed. Lung tissue was heated in a thermostatic oven at 60 ℃ for 48 h and then weighed to determine the baseline dry weight of lung.

Bronchoalveolar lavage fluid (BALF) analysis

BALF was collected by intratracheal administration of 1ml PBS into the lung and pumped back and forth gently for 3 times. The BALF was centrifuged (1500 rpm, 10 min, 4 ℃) to pellet the cells. The total cells were resuspended in 100 μl PBS, then neutrophils were identified and numbers quantified by Wright-Giemsa staining. Protein concentration in the supernatant was measured by BCA protein assay kit. Levels of TNF-α, IL-1β and IL-6 in the supernatant were quantified using ELISA kit from Neobioscience (Shenzhen, China) according to the manufacturer's instructions.

Assessment of MPO activity

MPO activity in the lung tissues was assessed with MPO assay kit according to the manufacturer's instructions Neobioscience (Shenzhen, China). Changes in OD value were measured at 460nm to calculate MPO activity.

TUNEL Staining

Lung tissues were fixed in 4% paraformaldehyde prior to paraffin embedding, and then cut into 4 μm sections. Then, terminal deoxynucleotidyl transferase dUTP nick-end labeling (TUNEL) staining was used to evaluate apoptosis rate as established method (50). Fluorescence staining was conducted using in situ Cell Death Detection Kit from Roche according to the manufacturer's instructions. The apoptotic cells were observed under light microscope and the results were expressed as the average number of TUNEL-positive staining cells per 100X magnification field.

Quantitative RT-PCR

Total RNA was extracted from mice lung tissues with Trizol reagent (Invitrogen, Carlsbad, CA) as described previously (51). Mouse-specific primers for Tumor Necrosis Factor-α (TNF-α), interleukin-1β (IL-1β), interleukin-6 (IL-6), and β-actin were purchased from Invitrogen (Carlsbad, CA). Total RNA was reversely transcribed to first strand cDNA using one-step RT kit (Takara Biotechnology, Dalian, CN) for one microgram sample. mRNA expression levels were determined using SYBR-Green Quantitative PCR Kit (Takara Biotechnology, Dalian, CN) on an ABI StepOne^{TM} real-time PCR system (Themo Fisher Scientific Inc., CA). The $2^{(-\Delta\Delta CT)}$method was used to determine the relative expression of mRNA. The amount of each gene was normalized to the amount of β-actin.

Western blotting

Western blotting was conducted as previous described (52), protein concentration was determined by BCA method. Briefly, protein content was separated on SDS-PAGE and transferred to PVDF membrane. The membrane was then blocked with 5% non-fat milk at room temperature for 2 h, following incubation with the primary antibodies against Bcl-2, Bax, cleaved caspase-3, ERK1/2, JNK, p38, TLR4 and TRPC6 (all from cell signaling, Boston, MA) at 4 ℃ overnight. Subsequently, the membrane was incubated with appropriated HRP-conjugated secondary antibody (cell signaling, Boston, MA) for 1 hour. GAPDH (Boster Biological Technology, Wuhan, CN) was used as loading

control. Target bands were developed using a chemiluminescence system and then visualized by exposure to Kodak X-ray film. Image J software was used for band densitometry .

Targeted fatty acids profiling of murine serum

300 μL of $CHCl_3$-MeOH (2:1, v/v) solution was added to 25 μL of plasma, vortexed for 30 s, and then mixed with 100 μL of ddH_2O and finally kept on ice for 5 min. The mixture was centrifuged at 10,000 rpm for 5 min at room temperature. 100 μL of the lower organic layer was drawn and dried with nitrogen blowing. The residues was dissolved with 150 μL of $CHCl_3$-MeOH（2:1, v/v） and derivatized by 40 μL of Meth-Prep II (Grace, USA) for 1 h at room temperature. A commercial fatty acids methyl esters mixture, F.A.M.E. Mix, (C4-C24, Supelco, USA) was used as standards.

Targeted fatty acids profiling of mice serum was carried on 7890B-5977B GC-MS (Agilent, MA, USA) with a DB-23 column (60 m × 0.25 mm × 0.15 μm, Agilent, MA, USA). The temperature programming was set to 50 ℃, 0.5 min → 50 ℃-140 ℃ (20 ℃/min), 5 min → 140 ℃-240 ℃ (4 ℃/min), 5 min. The auxiliary temperature was 240 ℃ and the injector temperature was 250 ℃ with 1.0 μL injection volume (10:1 split ratio). The helium carrier gas flow rate was set at 1 mL/min. MS detection was used selective ion scanning m/z 40-500 amu. The EI source temperature was 230 ℃. The MS quadrupole temperature were maintained at 150 ℃.

Non-targeted metabolic profiling of mice serum

50 μL of mice's plasma was mixed with 10 μL of nonadecanoic acid methanol solution (1 mg/mL, w/v) and 250 μL of H_2O-MeOH-$CHCl_3$ solution (2:5:2, v/v/v), then stayed at 4 ℃ for 20 min. The mixture was next centrifuged at 14,000 rpm for 15 min at room temperature. 200 μL of supernatant was taken and dried in nitrogen, which was followed by mixed with 80 μL of methoxyamine pyridine solution (15 mg/mL, w/v) and incubated at 37 ℃ for 90 min. Finally, 80 μL of bis-(trimethylsilyl) trifluoroacetamide (BSTFA) with 1% chlorotrimethyl-silane (TMCS) was added and incubated at 70 ℃ for 1 h. Nonadecanoic acid was used as internal standard substance.

The metabolic profiling was performed on 7890B-5977B GC-MS with a HP-5MS column (60 m × 0.25 mm × 0.25 μm, Agilent, MA, USA). The temperature was programmed to 60 ℃, 1 min → 60 ℃-100 ℃ (8 ℃/min), 5 min → 100 ℃-170 ℃ (15 ℃/min), 5 min → 170 ℃-210 ℃ (10 ℃/min), 5 min → 210 ℃-350 ℃ (10 ℃/min), 5 min. The auxiliary temperature was 240 ℃. The injector

temperature was 250 ℃ and injection volume was 1.0 μL. The helium carrier gas flow rate was set at 1 mL/min. MS detection was used selective ion scanning m/z 50-600 amu. The EI source was 230 ℃. The MS quadrupole were maintained at 150 ℃.

Data processing of GC-MS metabolic analysis

The total ion chromatogram (TIC) of GC-MS analysis were processed with Masshunter workstation B.07.00 (Agilent Technologies Co., Ltd, USA) for search and identification of compounds in NIST14.L database. The peaks of metabolites were detected, aligned and quantified by being imported to Quantitative Analysis (MS) (Agilent Technologies Co., Ltd, USA), which then were normalized by reference substances or internal standard.

Statistical analysis

All data are expressed as means ± standard deviation (SD). A Student's t-test was carried out and $P < 0.05$ was considered statistically significant. The principal component analysis (PCA) and partial least-squares discriminant analysis (PLS-DA) were performed on Simca-p 11.0 (Umetrics, Umeå, Sweden). Graphpad Prism 6.0 software (GraphPad, CA, USA) was used for graphics.

Molecular network construction using IPA

Construction of the metabolic interaction network among differential metabolites were performed on Ingenuity Pathways Analysis (IPA, QIAGEN, Germany). IPA is a web-based software application (http://www.ingenuity.com) that identifies biological pathways and functions relevant to biomolecules of interest. The list of modulated metabolites and their KEGG identification upon LPS or ACGs treatment were uploaded to IPA with the corresponding fold change to display molecular interaction networks as described before (22,23,24). Interactions among metabolites were generated based on the Ingenuity Pathway Knowledge Data Base. For correlations, a network score was based on the hypergeometric distribution and was calculated with the right-tailed Fisher's Exact Test. High scores indicate more relevant interactions for the network construction.

Author contributions

K. L.,Y. L. and J. G. designed the experiments. Y. L., Z. H. , K. L. and T.P. performed most of experiments and analyzed the data. Other authors assisted in experiments and discussed the results. K.

L., Y. L. and Z. H. wrote the manuscript. M. P. discussed the results and revised and improved the manuscript.

Acknowledgments

The work was supported in part by the National Natural Science Foundation of China [grant number 31300273], the Science and Technology Planning Project of Guangdong Province, China [grant number 2015A030302082], the Scientific Research Foundation for the Returned Overseas Chinese Scholars, State Education Ministry, China[grant number 20151098], the International Science and Technology Cooperation Project of Guangdong Province, China[grant number 2015A050502050,2016B050501003].

Conflict of Interest

The authors declare no conflict of interest.

REFERENCE AND NOTES

1 Li, C.; Yang, D.; Cao, X.; Wang, F.; Jiang, H.; Guo, H.; Du, L.; Guo, Q.; Yin, X. LFG-500, a newly synthesized flavonoid, attenuates lipopolysaccharide-induced acute lung injury and inflammation in mice. *Biochem Pharmacol*. **113**:57-69; 2016.

2 Zhao, Z.; Tang, X.; Zhao, X.; Zhang, M.; Zhang, W.; Hou, S.; Yuan, W.; Zhang, H.; Shi, L.; Jia, H.; Liang, L.; Lai, Z.; Gao, J.; Zhang, K.; Fu, L.; Chen, W. Tylvalosin exhibits anti-inflammatory property and attenuates acute lung injury in different models possibly through suppression of NF-κB activation. *Biochem Pharmacol*. **90**:73-87; 2014.

3 Wan, L.; Meng, D.; Wang, H.; Wan, S.; Jiang, S.; Huang, S.; Wei, L.; Yu, P. Preventive and therapeutic effects of thymol in a lipopolysaccharide-induced acute lung injury mice model. *Inflammation*.**41**:183-192; 2018.

4 Ding, N.; Wang, F.; Xiao. H; Xu, L.; She, S. Mechanical ventilation enhances HMGB1 expression in an LPS-induced lung injury model. *PLoS ONE*. **8**:e74633; 2013.

5 Sato, K.; Kadiiska, M.B.; Ghio, A.J.; Corbett, J.; Fann, Y.C.; Holland, S.M.; Thurman, R.G.; Mason, R.P. *In vivo* lipid-derived free radical formation by NADPH oxidase in acute lung injury induced by lipopolysaccharide: a model for ARDS. *FASEB J*. **16**:1713-1720; 2002.

6 Goodman, R.B.; Pugin, J.; Lee, J.S.; Matthay, M.A. Cytokine-mediated inflammation in acute lung injury. *Cytokine Growth Factor Rev*. **14**:523-535; 2003.

7 Martin, T.R. Cytokines and the acute respiratory distress syndrome (ARDS): a question of balance. *Nat Med*. **3**:272-273; 1997.

8 Boonstra, A.; Rajsbaum, R.; Holman, M.; Marques, R.; Asselin-Paturel, C.; Pereira, J.P.; Bates, E.E.; Akira, S.; Vieira, P.; Liu, Y.J.; Trinchieri, G.; O'Garra, A. Macrophages and Myeloid Dendritic Cells, but Not Plasmacytoid Dendritic Cells, Produce IL-10 in Response to MyD88- and TRIF-Dependent TLR Signals, and TLR-Independent Signals. *J Immunol*. **177**:7551-7558; 2006.

9 Malczyk, M.; Erb, A.; Veith, C.; Ghofrani, H.A.; Schermuly, R.T.; Gudermann, T.; Dietrich, A.; Weissmann, N.; Sydykov, A. The Role of Transient Receptor Potential Channel 6 Channels in the pulmonary vasculature. *Front Immunol*. **8**:707; 2017.

10 Tauseef, M.; Knezevic, N.; Chava, K.R.; Smith, M.; Sukriti, S.; Gianaris, N.; Obukhov, A.G.; Vogel, S.M.; Schraufnagel, D.E.; Dietrich, A.; Birnbaumer, L.; Malik, A.B.; Mehta, D. TLR4 activation of TRPC6-dependent calcium signaling mediates endotoxin-induced lung vascular permeability and inflammation. *J Exp Med*. **209**:1953-1968; 2012.

11 Wheeler, A.P.; Bernard, G.R. Acute lung injury and the acute respiratory distress syndrome: a clinical review. *Lancet*. **369**:1553-1564; 2007.

12 Matthay, M.A.; Ware, L.B.; Zimmerman, G.A. The acute respiratory distress syndrome. *J Clin Invest*. **122**:2731-2740; 2012.

13 Imai, Y.; Kuba, K.; Neely, G.G.; Yaghubian-Malhami, R.; Perkmann, T.; van Loo, G.; Ermolaeva, M.; Veldhuizen, R.; Leung, Y.H.; Wang, H.; Liu, H.; Sun, Y.; Pasparakis, M.; Kopf, M.; Mech, C.; Bavari, S.; Peiris, J.S.; Slutsky, A.S.; Akira, S.; Hultqvist, M.; Holmdahl, R.; Nicholls, J.; Jiang, C.; Binder, C.J.; Penninger, J.M. Identification of oxidative stress and Toll-like receptor 4 signaling as a key pathway of acute lung injury. *Cell*. **133**:235-249; 2008.

14 National Pharmacopoeia Committee. Pharmacopoeia of People's Republic of China. Beijing: Chemical Industry Press. 2015(Vol. 1):95; 2015.

15 Chen, Y.F.; Yang, C.Y.; Li K.P.; Zeng, Y.; Wang, Y.F. Protection of total flavones from *Microcos paniculata* on acute myocardial ischemia in rats and its mechanism. *Chinese Traditional & Herbal Drugs*. **44**:1003-1007; 2013.

16 Lee, W.; Ku, S.K.; Bae, J.S. Vascular barrier protective effects of orientin and isoorientin in LPS-induced inflammation *in vitro* and *in vivo*. *Vascul Pharmacol*. **62**:3-14; 2014.

17 Francisco, V.; Figueirinha, A.; Costa, G.; Liberal, J.; Lopes, M.C.; García-Rodríguez, C.; Geraldes C.F.G.C.; Cruz, M.T.; Batista, M.T. Chemical characterization and anti-inflammatory activity of luteolin glycosides isolated from lemongrass. *J Funct Foods*. **10**:436-443; 2014.

18 Chen, M.; Wang, T.; Jiang, Z.Z.; Shan, C.; Wang, H.; Wu, M.J.; Zhang, S.; Zhang, Y.; Zhang, L.Y. Anti-inflammatory and hepatoprotective effects of total flavonoid C-glycosides from *Abrus mollis* extracts. *Chin J Nat Med*. **12**:590-598; 2014.

19 Wang, Y.; Jiang, Z.Z.; Chen, M.; Wu, M.J.; Guo, H.L.; Sun, L.X.; Wang, H.; Zhang, S.; Wang, T.; Zhang, L.Y. Protective effect of total flavonoid C-glycosides from *Abrus mollis* extract on lipopolysaccharide-induced lipotoxicity in mice. *Chin J Nat Med*. **12**:461-468; 2014.

20 Klupczyńska, A.; Dereziński, P.; Kokot, Z.J. Metabolomics in medical sciences-trends, challenges and perspectives. *Acta Pol Pharm*. **72**:629-641; 2015.

21 Patti, G. J.; Yanes, O.; Siuzdak, G. Metabolomics: the apogee of the omic triology. *Nat Rev Mol Cell Biol*. **13**:263-269; 2011.

22 Chu, Y.; Jiang, H.; Ju, J.; Li, Y.; Gong, L.; Wang, X.; Yang, W.; Deng, Y. A metabolomic study using HPLC-TOF/MS coupled with ingenuity pathway analysis: Intervention effects of *Rhizoma Alismatis* on spontaneous hypertensive rats. *J Pharm Biomed Anal*. **117**:446-452; 2016.

23 Shen, P.; Hu, Q.; Dong, M.; Bai, S.; Liang, Z.; Chen, Z.; Li, P.; Hu, Z.; Zhong, X.; Zhu, D.; Wang, H.; Xie, P. Venlafaxine exerts antidepressant effects possibly by activating MAPK-ERK1/2 and P13K-AKT pathways in the hippocampus. *Behav Brain Res*. **335**:63-70; 2017.

24 Su, T.; Tan, Y.; Tsui, M.S.; Yi, H.; Fu, X.Q.; Li, T.; Chan, C.L.; Guo, H.; Li, Y.X.; Zhu, P.L.; Tse A.K.; Cao, H.; Lu, A.P.; Yu, Z.L. Metabolomics reveals the mechanisms for the cardiotoxicity of *Pinelliae Rhizoma* and the toxicity-reducing effect of processing. *Sci Rep*. **6**:34692; 2016.

25 Matute-Bello, G.; Frevert, C.W.; Martin, T.R. Animal models of acute lung injury. *Am J Physiol Lung Cell Mol Physiol*. **295**:L379-L399; 2008.

26 Wang, L.; Ye, Y.; Su, H.B.; Yang, J.P. The anesthetic agent sevoflurane attenuates pulmonary acute lung injury by modulating apoptotic pathways. *Braz J Med Biol Res*. **50**:e5747; 2017.

27 Ogata-Suetsugu, S.; Yanagihara, T.; Hamada, N.; Ikeda-Harada, C.; Yokoyama, T.; Suzuki, K.; Kawaguchi, T.; Maeyama, T.; Kuwano, K.; Nakanishi, Y. Amphiregulin suppresses epithelial cell apoptosis in lipopolysaccharide-induced lung injury in mice. *Biochem Biophys Res Commun*. **484**:422-428; 2017.

28 Szarka, R.J.; Wang, N.; Gordon, L.; Nation, P.N.; Smith, R.H. A murine model of pulmonary damage induced by lipopolysaccharide via intranasal instillation. *J Immunol Methods*. **202**:49-57; 1997.

29 Johnson, E.R.; Matthay, M.A. Acute lung injury: epidemiology, pathogenesis, and treatment. *J Aerosol Med Pulm Drug Deliv*. **23**:243-252; 2010.

30 Chudow, M.; Carter, M.; Rumbak, M. Pharmacological treatments for acute respiratory distress syndrome. *AACN Adv Crit Care*. **26**:185-191; 2015.

31. Abraham, E. Neutrophils and acute lung injury. *Crit Care Med*. **31**(Suppl. 4):S195-S199; 2003.

32 Chignard, M.; Balloy, V. Neutrophil recruitment and increased permeability during acute lung injury induced by lipopolysaccharide. *Am J Physiol Lung Cell Mol Physiol*. **279**:1083-1090; 2000.

33 Steinberg, K.P.; Milberg, J.A.; Martin, T.R.; Maunder, R.J.; Cockrill, B.A.; Hudson, L.D. Evolution of bronchoalveolar cell populations in the adult respiratory distress syndrome. *Am J Respir Crit Care Med*. **150**:113-122; 1994.

34 Chopra, M.; Reuben, J.S.; Sharma, A.C. Acute lung injury: apoptosis and signaling mechanisms. *Exp Biol Med (Maywood)*. **234**:361-371; 2009.

35 Youm Y.H.; Nguyen, K.Y.; Grant, R.W, Goldberg, E.L.; Bodogai, M.; Kim, D.; D'Agostino, D.; Planavsky, N.; Lupfer, C.; Kanneganti, T.D.; Kang, S.; Horvath, T.L.; Fahmy, T.M.; Crawford, P.A.;

Biragyn, A.; Alnemri, E.; Dixit, V.D. The ketone metabolites β-hydroxybutyrate blocks NLRP3 inflammasome-mediated inflammatory disease. *Nat Med*. **21**:263-269; 2015.

36 Wang, X.; Liu, Y.; Li, S.; Pi, D.; Zhu, H.; Hou, Y.; Shi, H.; Leng, W. Asparagine attenuates intestinal injury, improves energy status and inhibits AMP-activated protein kinase signalling pathways in weaned piglets challenged with *Escherichia coli* lipopolysaccharide. *Br J Nutr.* **114**:553-565; 2015.

37 Fallahzadeh, M.K.; Namazi, M.R.; Gupta, R.C. Taurine: a potential novel addition to the anti-systemic sclerosis weaponry. *Arch Med Res*. **41**:59-61; 2010.

38 Su, Y.; Fan W, Ma Z, Wen, X.; Wang, W.; Wu. Q.; Huang, H. Taurine improves functional and histological outcomes and reduces inflammation in traumatic brain injury. *Neuroscience*. **266**:56-65; 2014.

39 Lv, H.; Yu, Z.; Zheng, Y.; Wang, L.; Qin, X.; Cheng, G.; Ci, X. Isovitexin exerts anti-Inflammatory and anti-oxidant activities on lipopolysaccharide-induced acute lung injury by inhibiting MAPK and NF-κB and activating HO-1/Nrf2 pathways. *Int J Biol Sci*. **12**:72-86; 2016.

40 Rosa, S.I.; Rios-Santos, F.; Balogun, S.O.; Martins, D.T. Vitexin reduces neutrophil migration to inflammatory focus by down-regulating pro-inflammatory mediators via inhibition of p38, ERK1/2 and JNK pathway. *Phytomedicine*. **23**:9-17; 2016.

41 Lucas, R.; Verin, A.D.; Black, S.M.; Catravas, J.D. Regulators of endothelial and epithelial barrier integrity and function in acute lung injury. *Biochem Pharmacol*. **77**:1763-1772; 2009.

42 Montell, C.; Rubin, G.M. Molecular characterization of the Drosophila trp locus: a putative integral membrane protein required for phototransduction. *Neuron*. **2**:1313-1323; 1989.

43 Montell, C.; Jones, K.; Hafen, E.; Rubin, G. Rescue of the Drosophila phototransduction mutation TRP by germline transformation. *Science*. **230**:1040-1043; 1985.

44 Matthay, M.A.; Ware, L.B.; Zimmerman, G.A. The acute respiratory distress syndrome. *J Clin Invest*. **122**:2731-2740; 2012.

45 Li, S.S.; Wu, J.; Chen, L.G.; Du, H.; Xu, Y.J.; Wang, L.J.; Zhang, H.J.; Zheng, X.C.; Wang, L.S. Biogenesis of C-glycosyl flavones and profiling of flavonoid glycosides in Lotus (*Nelumbo nucifera*).

PLoS One. **9**:e108860; 2014.

46 Liu, C.L.; Lin, S.; He, Z.R.; Huang, Y.H.; Li K.P. Simultaneous determination of eight flavone glycosides in total flavonoids fraction of *Microcos paniculata* using quantitative analysis of multi-components by single marker method. *Chinese Traditional & Herbal Drugs*. **48**:1872-1877; 2017.

47 Kilkenny, C.; Browne, W.; Cuthill, I.C.; Emerson, M.; Altman, D.G.; NC3Rs Reporting Guidelines Working Group. Animal research: reporting in vivo experiments: the ARRIVE guidelines. *J Gene Med*. **12**:561-563; 2010.

48 McGrath, J.C.; Drummond, G.B.; McLachlan, E.M.; Kilkenny, C.; Wainwright, C.L. Guidelines for reporting experiments involving animals: the ARRIVE guidelines. *Br J Pharmacol*. **160**:1573-1576; 2010.

49 Gong, J.; Wu, Z.Y.; Qi, H.; Chen, L.; Li, H.B.; Li, B.; Yao, C.Y.; Wang, Y.X.; Wu, J.; Yuan, S.Y.; Yao, S.L.; Shang, Y. Maresin 1 mitigates LPS-induced acute lung injury in mice. *Br J Pharmacol*. **171**:3539-3550; 2014.

50 Wu, X.Q.; He, L.S.; Chen, F.J.; He, X.E.; Cai, Y.; Zhang G.P.; Yi, Q.; He, M.X.; Luo, J.D. Impaired autophagy contributes to adverse cardiac remodeling in acute myocardial infarction. PLoS One.**9**:e112891. 2014.

51 Cai, Y.; Ma, W.Q.; Xiao, Y.C.; Wu, B.; Li, X.B.; Liu, F.R.; Qiu, J.H.; Zhang, G.S. High doses of baicalin induces kidney injury and fibrosis through regulating TGF-β/Smad signaling pathway. *Toxicol Appl Pharmacol*. **333**:1-9. 2017.

52 Liu, Y.; Gao, M.; Ma, M.M.; Tang, Y.B.; Zhou, J.G.; Wang, G.L.; Du, Y.H.; Guan, Y.Y. Endophilin A2 protects H_2O_2-induced apoptosis by blockade of Bax translocation in rat basilar artery smooth muscle cells. *J Mol Cell Cardiol*. **92**:122-133; 2016.

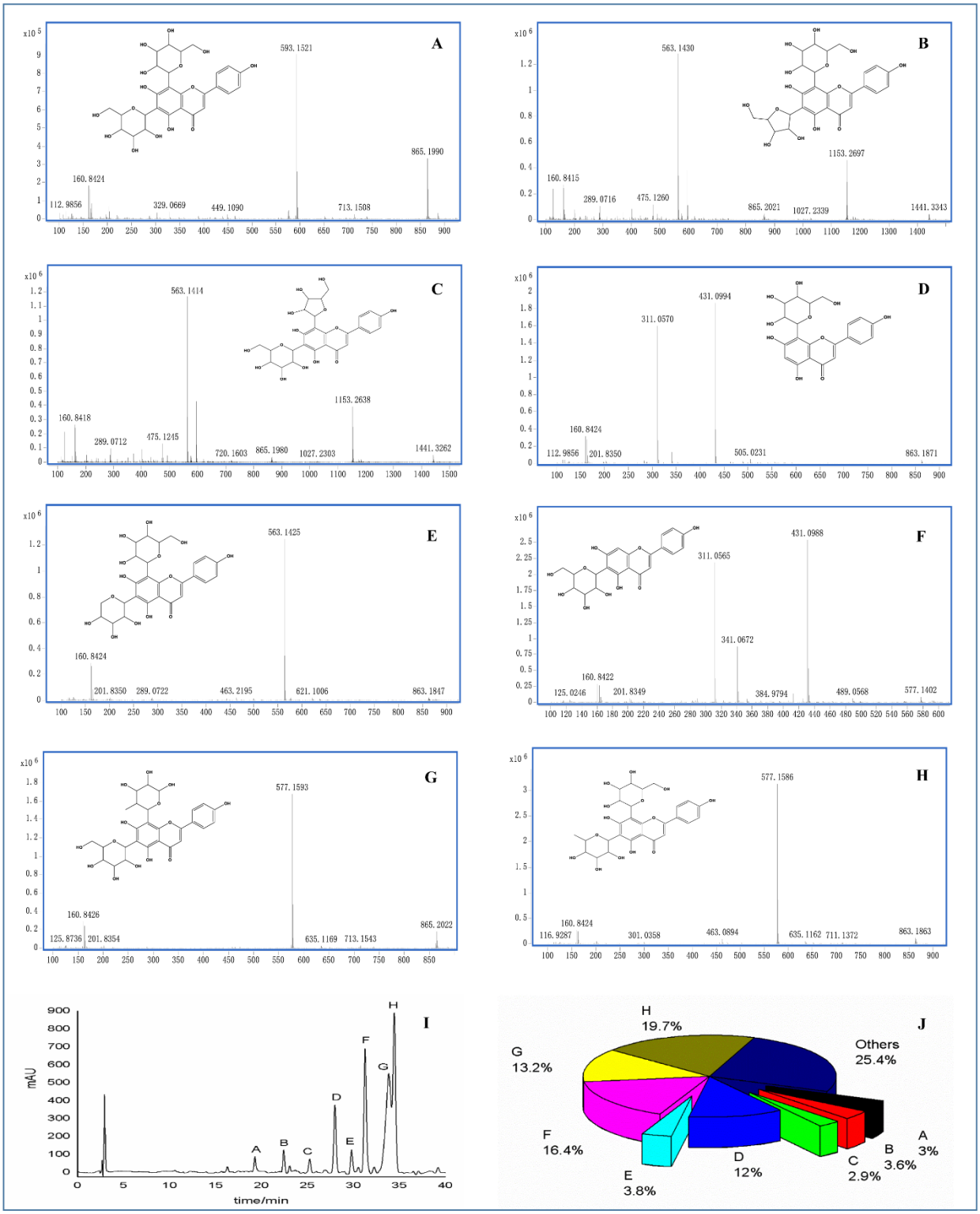

Figure 1. Qualitative and quantitative profiling of *Microcos paniculata* apigenin C-glycosides (ACGs) fractions. (**A**) vicenin-2, (**B**) isoshaftoside, (**C**) shaftoside, (**D**) vitexin, (**E**) vicenin-1, (**F**) isovitexin, (**G**) violanthin, (**H**) isoviolanthin, (**I**) HPLC chromatography of *M. paniculata* ACGs fractions. (**J**) Content of eight compounds in *M. paniculata* ACGs fractions by HPLC analysis.

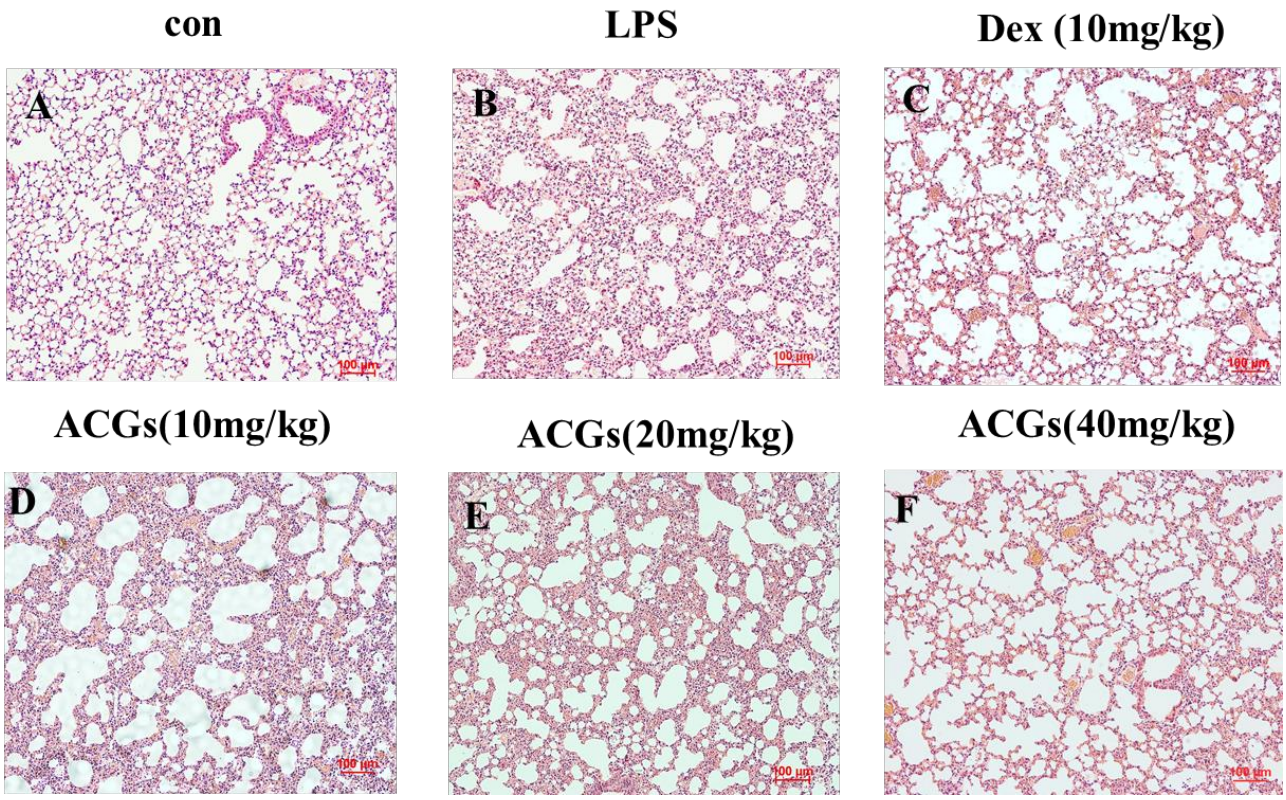

Figure 2. ACGs ameliorated LPS-mediated lung histopathologic changes. Lung tissue sections were stained with hematoxylin and eosin (H&E) for histopathology analysis (magnification 100×). **(A)** PBS group, **(B)** LPS group, **(C)** LPS and dexamethasone (10 mg/kg) group, **(D)** LPS and ACGs (10 mg/kg) group, **(E)** LPS and ACGs (20 mg/kg) group, **(F)** LPS and ACGs (40 mg/kg) group. Pathological changes in the treated groups were virtually indistinguishable from those with PBS group mice（n=6 mice per group).

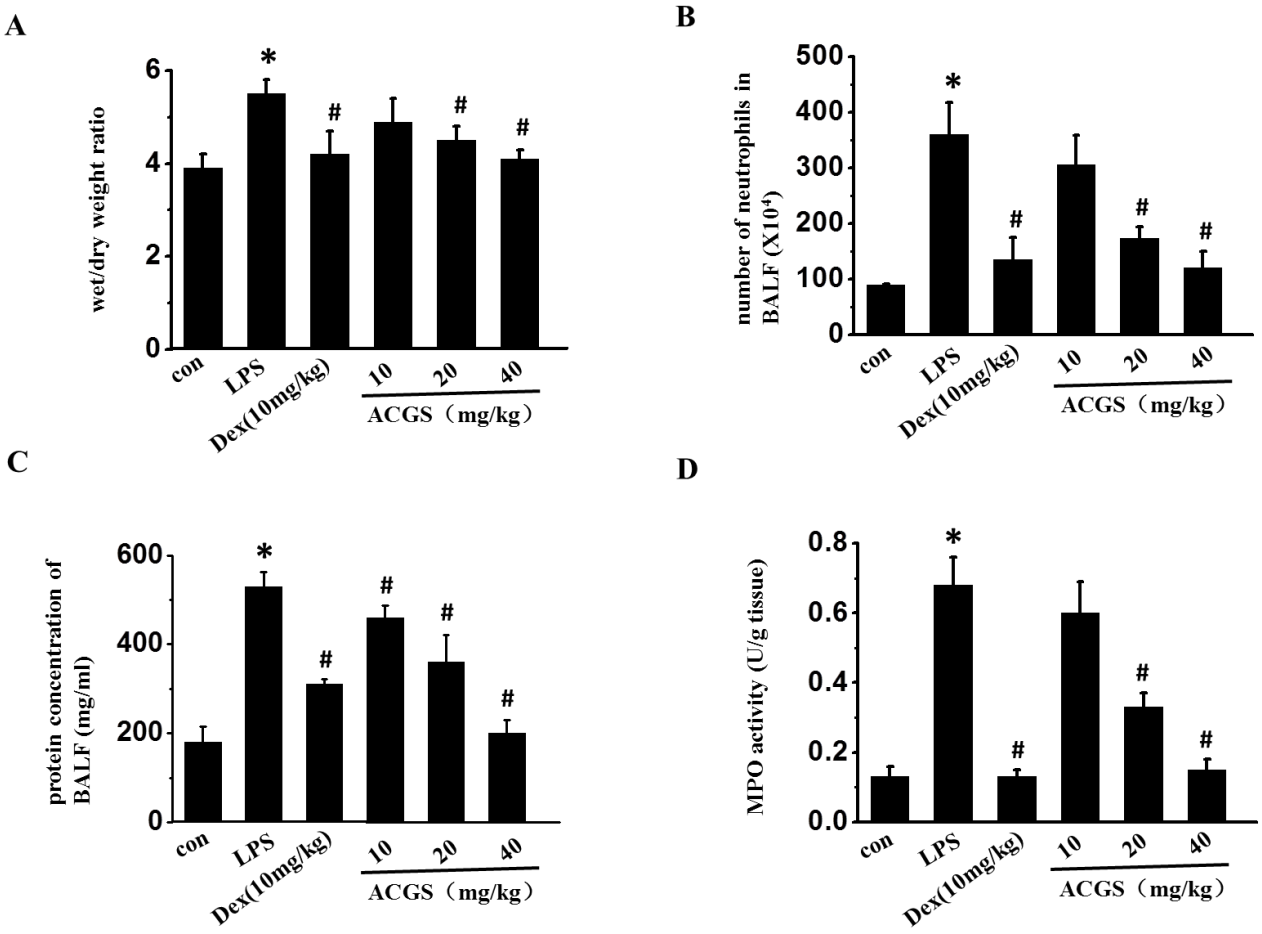

Figure 3. ACGs relieved LPS-induced pulmonary edema and microvascular permeability. (**A**) Dissected lung tissues were weighed and oven dried at 60 ℃ for 24 h for calculation of wet/dry ratio. (**B**) Neutrophils in the BALF were observed by cell smears (Wright-Giemsa staining) and counts. (**C**) The total protein concentration in supernatant was measured by BCA method. (**D**) MPO activity in lung tissue. Intranasal instillation of LPS (2mg/kg) resulted in significantly increased wet/dry ratio and BALF neutrophils number, protein concentration as well as pulmonary MPO activity, which were markedly attenuated by ACGs treatment (n=6 mice per group, * $P<0.05$ vs con group; #$P<0.05$ vs LPS treated group).

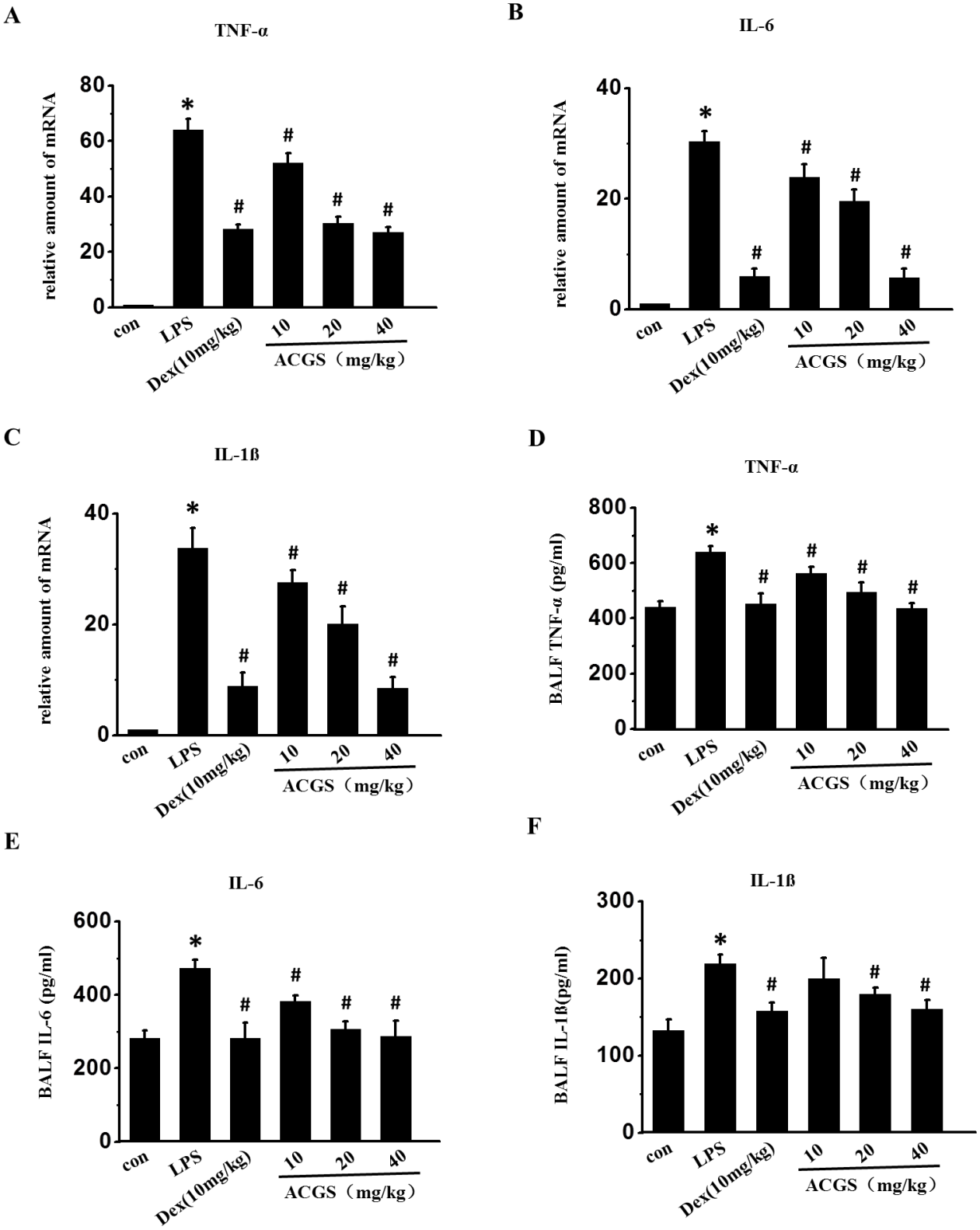
A
TNF-α
relative amount of mRNA
80
60
40
20
0
con
LPS
Dex(10mg/kg)
10
20
40
ACGS（mg/kg）
B
IL-6
relative amount of mRNA
40
20
0
C
IL-1ß
relative amount of mRNA
40
20
0
D
TNF-α
BALF TNF-α (pg/ml)
800
600
400
200
0
E
IL-6
BALF IL-6 (pg/ml)
600
400
200
0
F
IL-1ß
BALF IL-1ß(pg/ml)
300
200
100
0

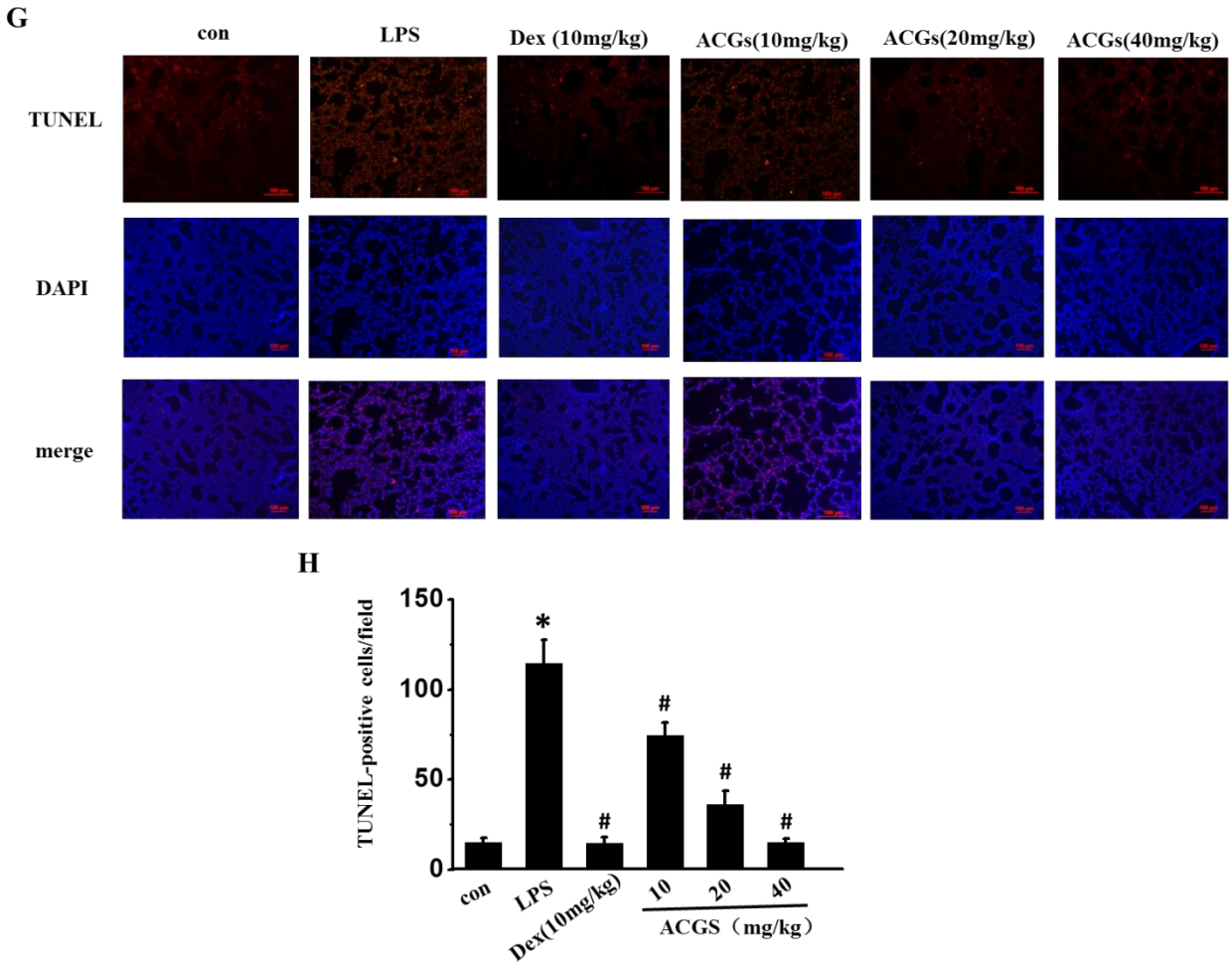

Figure 4. ACGs attenuated lung inflammation and apoptosis in LPS-induced ALI in mice. ACGs reduced the mRNA expression of pro-infammatory cytokines, such as TNF-α **(A)**, IL-6 **(B)**, and IL-1β **(C)**. And moreover, ACGs reduced pro- infammatory cytokines level, including TNF-α **(D)**, IL-6 **(E)** and IL-1β **(F)**. Data are expressed as mean ± SD (n = 6 mice per group, * P<0.05 vs con group; #P<0.05 vs LPS treated group). **(G)** The lung tissues were subjected to the TUNEL staining. TUNEL positive cells were indicated by arrows (magnification 100X). **(H)** Densitometric analysis showed that the quantity of TUNEL-positive cells was elevated in LPS group mice, and ACGs signifcantly reduced it (n=6 mice per group, * P<0.05 vs con group; #P<0.05 vs LPS treated group).

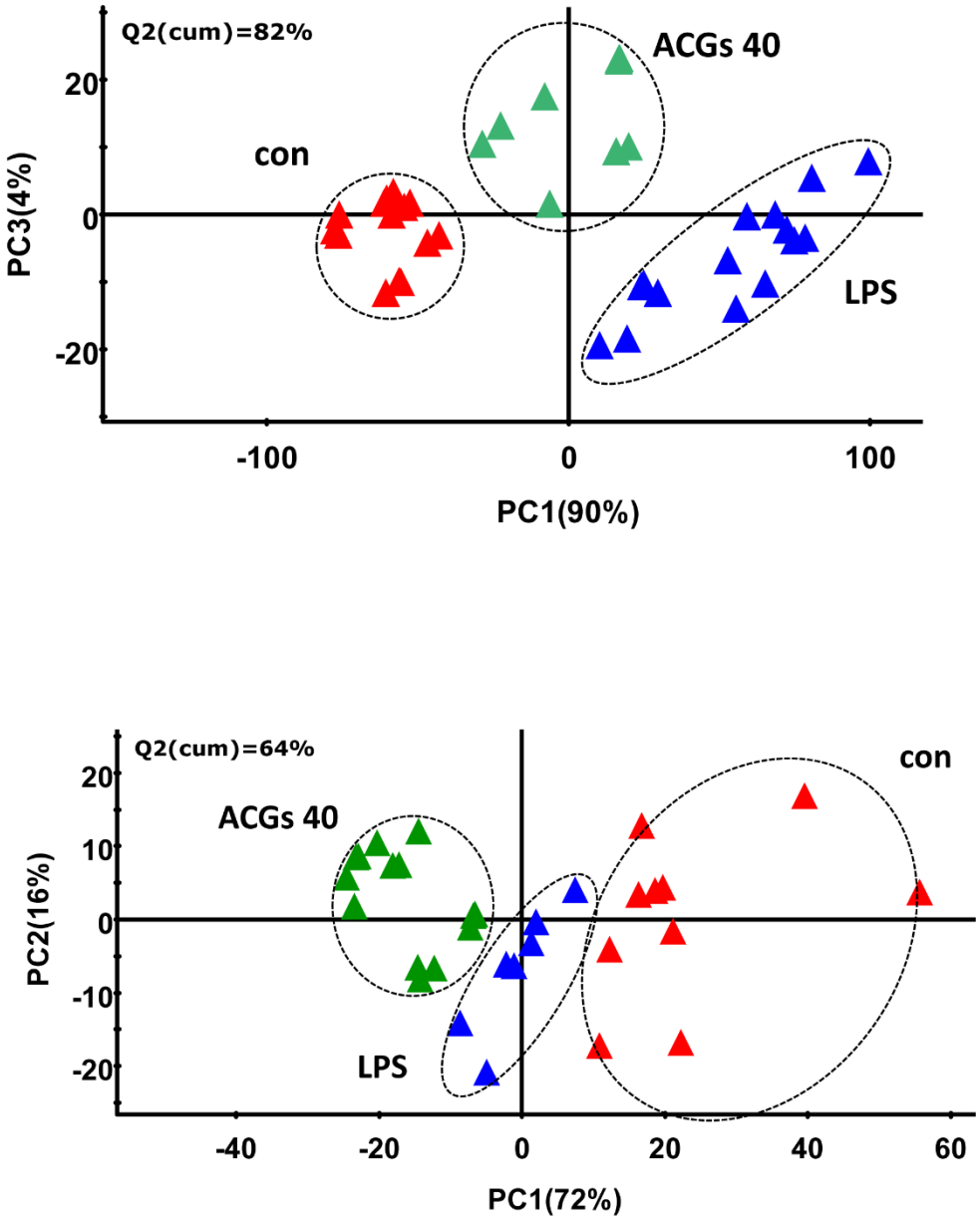

Figure 5. The pattern recognition analysis of metabolites among control group, LPS group and ACGs group (40 mg/kg). (A) The PCA analysis of targeted fatty acids [$R^2X(cum) = 0.9807$, $Q^2(cum) = 0.8223$]. **(B)** The PCA analysis of water-soluble metabolites [$R^2X(cum) = 0.8845$, $Q^2(cum) = 0.6447$]. **"con",** control group, which was in red triangles; **"LPS",** LPS group, which was presented by blue triangles; **"ACGs 40",** apigenin C-glycosides group (40 mg/kg), which was showed in green triangles.

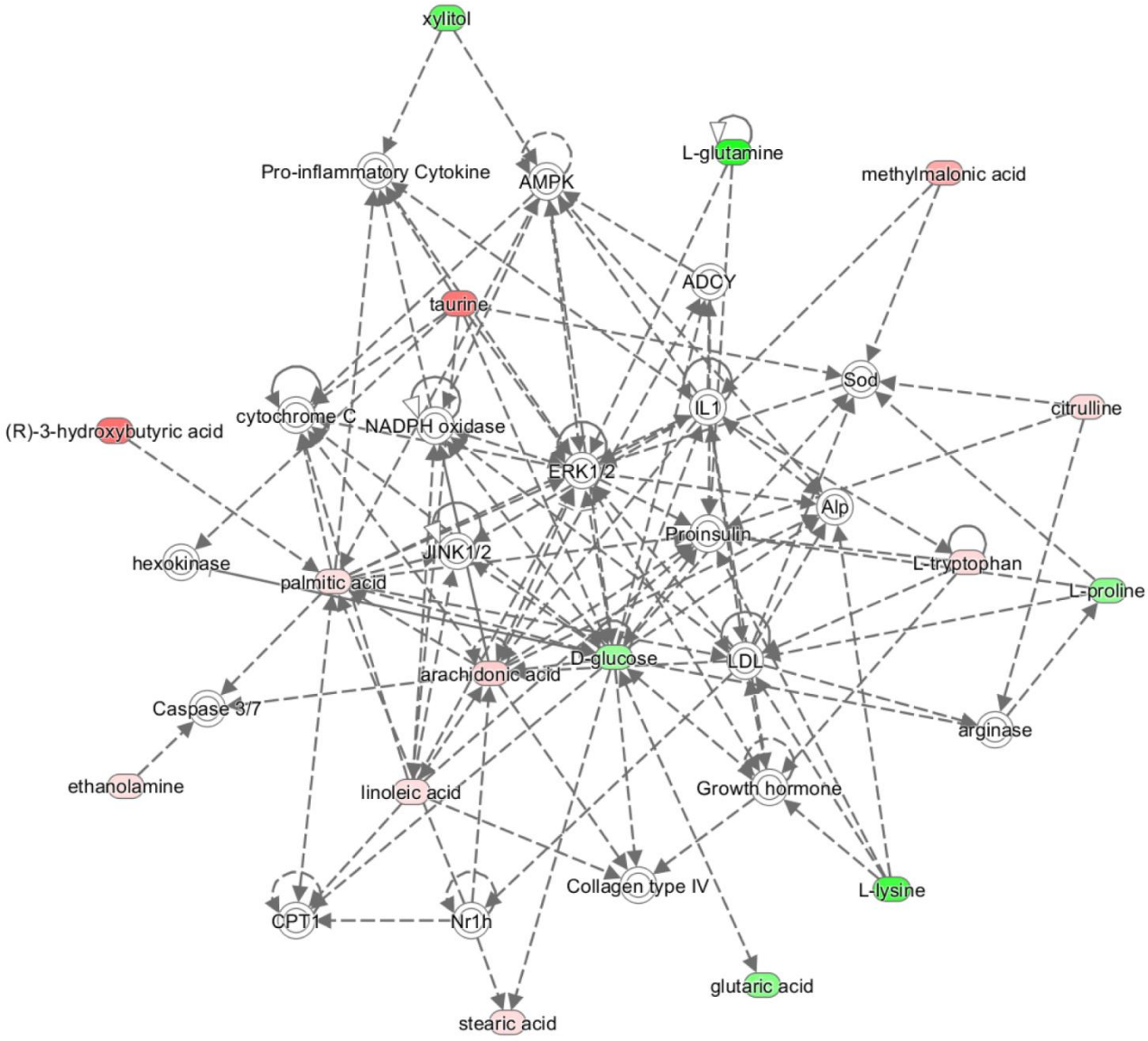

Figure 6. Ingenuity Pathway Analysis (IPA) generated top regulated molecular interaction network in LPS-induced ALI versus high-dose ACGs (40 mg/kg) treated mice. The top regulated metabolic network in LPS group versus ACGs group included "cellular compromise, lipid metabolism, small molecule biochemistry" (IPA score 43). The compounds in red were increased in ACGs group (40 m/kg) compared with LPS group; while those in green were decreased in ACGs group (40 m/kg) compared with LPS group.

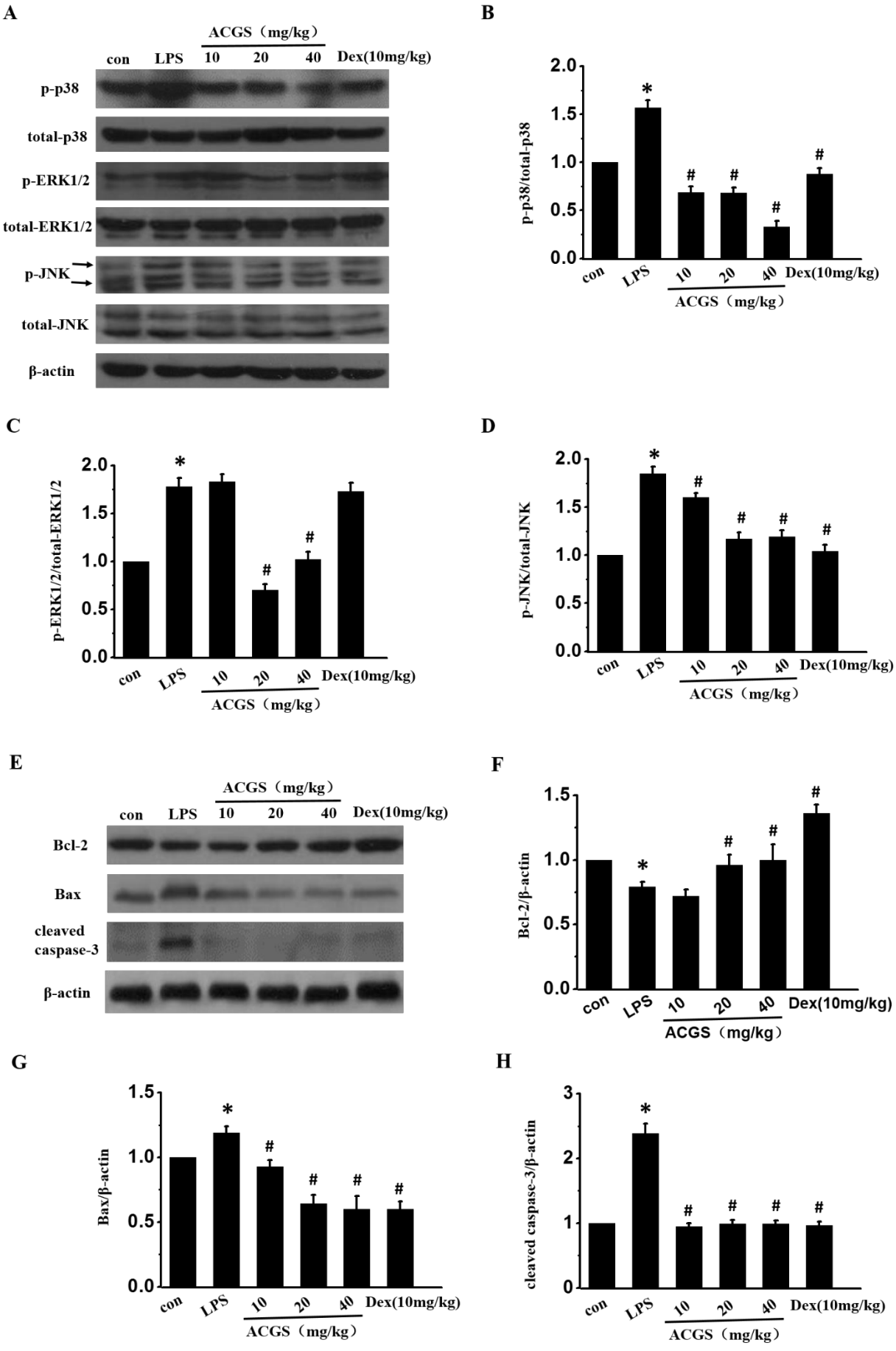
A
ACGS（mg/kg）
con
LPS
10
20
40
Dex(10mg/kg)
p-p38
total-p38
p-ERK1/2
total-ERK1/2
p-JNK
total-JNK
β-actin
B
p-p38/total-p38
C
p-ERK1/2/total-ERK1/2
D
p-JNK/total-JNK
E
Bcl-2
Bax
cleaved caspase-3
β-actin
F
Bcl-2/β-actin
G
Bax/β-actin
H
cleaved caspase-3/β-actin

Figure 7. ACGs attenuated lung inflammation and apoptosis through MAPKs pathway and mitochondrial pathway respectively. (A-D) Western Blot showed that the phosphorylation of p38, ERK1/2 and JNK increased by treatment of LPS, indicating that MAPK pathway was activated. ACGs attenuated the phosphorylation of p38, ERK1/2 and JNK induced by LPS (n=5, **P*<0.05 vs. con group; #P<0.05 vs LPS treated group). **(E-H)** Western Blot results showed the effects of ACGs on LPS-induced Bcl-2, Bax and cleaved caspase-3 expression. Densitometric analysis showed that LPS decreased the expression of Bcl-2 and increased the expression of Bax and cleaved caspase-3, which was reversed by ACGs treatment (n=5, **P*<0.05 vs. con group; #P<0.05 vs LPS treated group).

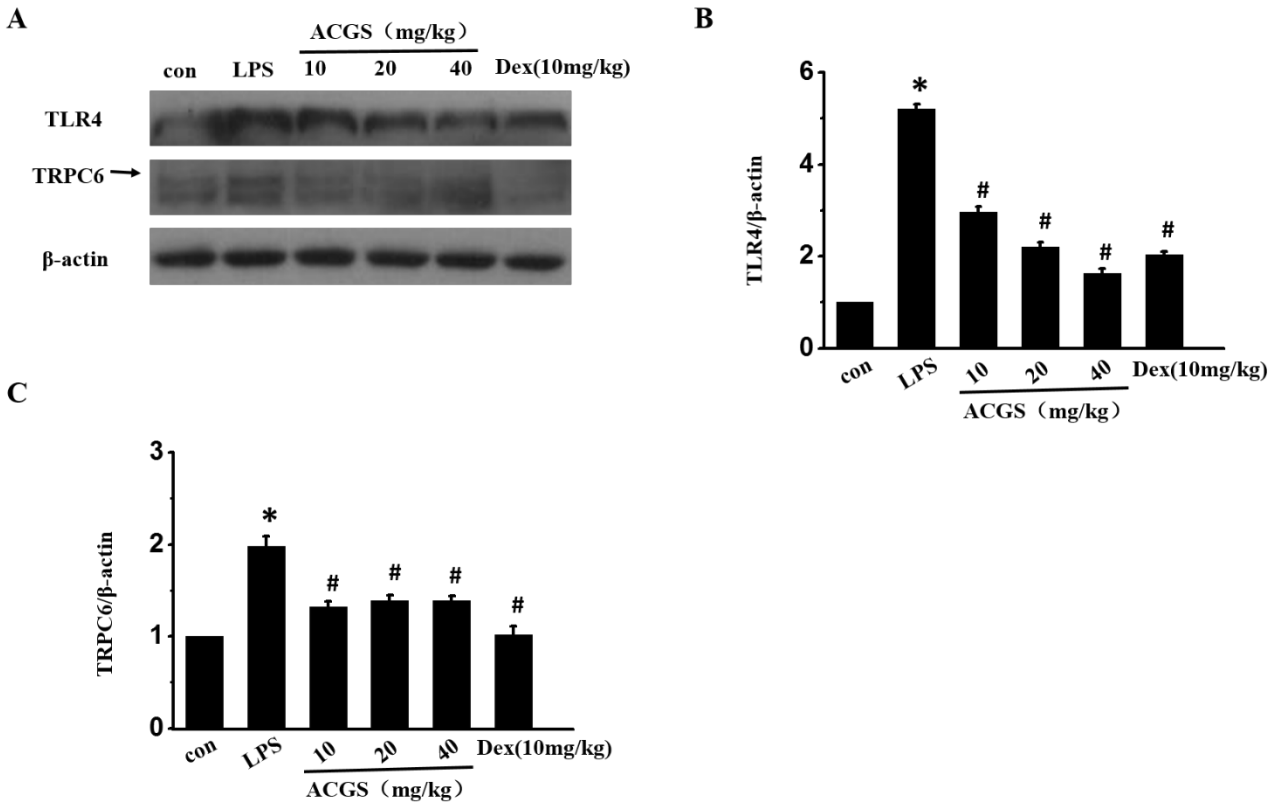

Figure 8. ACGs protects LPS-induced apoptosis and inflammation via modulating TLR4-TRPC6 pathway. (A-C) Western Blot showed that TLR4 and TRPC6 obviously increased after LPS treatment. While ACGs suppressed the expression of TLR4 and TRPC6 induced by LPS (n=5, **P*<0.05 vs. con group; #P<0.05 vs LPS treated group).

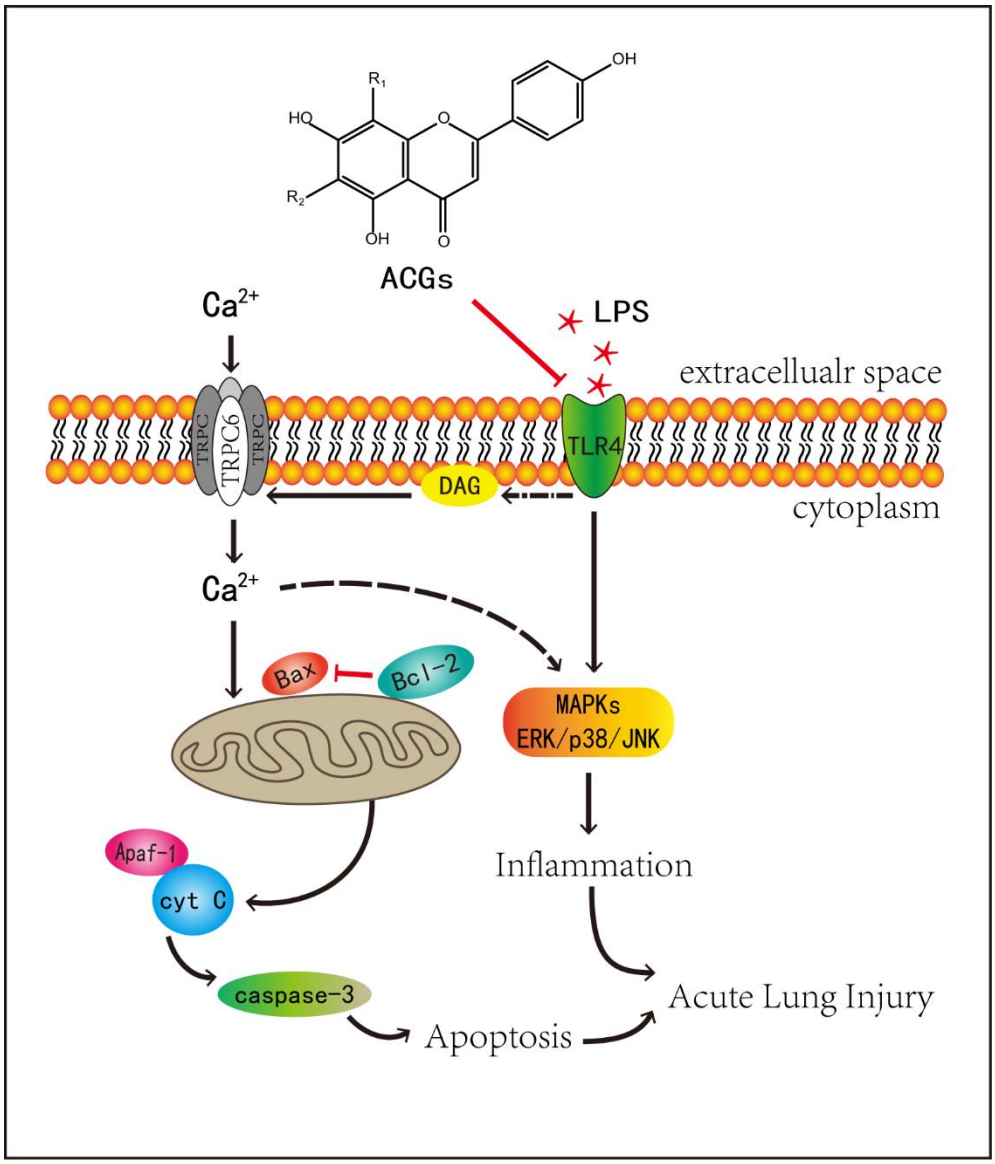

Figure 9. Proposed underlying mechanisms for ACGs protects acute inflammation and apoptosis in LPS-induced acute lung injury by suppressing activation of TLR4 /TRPC6 signaling pathway. ACGs, apigenin C-glycosides; DAG, diacylglycerol; Ca^{2+}, calcium ion ligand; LPS, lipopolysaccharide; TLR4, toll-like receptor 4; TRPC6, classical transient receptor potential channel 6; MAPKs, mitogen-activated protein kinase; ERK, extracellular regulated protein kinase; JNK, c-Jun N-terminal kinase; Bax, Bcl-2-Associated X, Bcl-2, B-cell lymphoma-2; cyt C, cytochrome C; Apaf-1, apoptotic protease activating factor-1. Solid arrows indicate direct interactions; dotted arrows illustrate indirect interactions.

Table 1 The significantly differential metabolites between LPS group and ACGs group (40 mg/kg) uncovered by metabolic profiling and multivariable statistical analysis

Compound name	Retention Time	base peak	p-value	VIP	fold change*	KEGG ID
Glyoxylic acid	11.906	73.05	0.001	1.6426	-1.0013	C00048
Tryptamine	12.713	174.09	0.000	1.8236	0.6173	C00398
Ethanolamine	12.914	147.05	0.001	1.6550	0.3973	C00189
3-Hydroxybutyric acid	15.678	147.05	0.008	1.3688	2.3498	C01089
L-Valine	16.754	144.11	0.003	1.5046	-0.5641	C00183
L-Isoleucine	18.224	158.12	0.017	1.2472	0.2886	C00407
Inosose	18.668	73.04	0.004	1.9233	-1.6772	C00691
Butanoic acid	20.708	73.03	0.005	1.4629	-1.1516	C00246
methylmalonic acid	21.865	73.05	0.018	1.3325	1.3800	C02170
Citrulline	22.866	73.03	0.030	1.1342	0.6167	C00327
Pentanedioic acid	24.179	73.04	0.015	1.6285	-1.4130	C00489
L-Proline	24.398	73.03	0.001	1.7222	-1.3367	C00148
D-Ribose	25.024	73.04	0.002	1.7902	-2.1364	C00121
Asparagine	26.075	73.04	0.026	1.8956	3.4141	C00152
Taurine	26.187	73.05	0.000	1.9151	2.2351	C00245
Arabinofuranose	26.294	217.1	0.000	2.0847	-2.9801	C06115
Xylitol	27.326	73.04	0.047	1.4590	-1.8963	C00379
DL-Ornithine	27.851	73.03	0.043	1.0856	-0.6714	C01602
L-Glutamine	28.252	73.04	0.003	1.9134	-2.6206	C00064
d-Glucose	31.654	319.16	0.000	1.9717	-1.1776	C00031
L-Lysine	31.736	73.04	0.026	1.5025	-2.2147	C00047
L-Tyrosine	32.061	218.11	0.011	1.3227	-0.6135	C00082
meso-Erythritol	33.25	73.04	0.007	1.0904	1.6997	C00503
Myo-Inositol	34.457	73.04	0.000	2.0698	-2.1534	C00137
L-Tryptophan	35.595	202.09	0.003	1.4872	0.6093	C00078
Doconexent	38.16	73.03	0.005	1.6802	0.8782	C06429
Palmitic acid	23.979	74.0	0.001	3.632	0.5055	C00249
Stearic acid	27.887	74.0	0.000	2.582	0.5382	C01530
Linoleic acid	29.332	67.0	0.000	2.810	0.5105	C01595
Arachidonic acid	33.706	79.0	0.000	2.182	0.7890	C00219

*fold change: $\log_2$(ACGs 40/LPS)

Supplemental materials

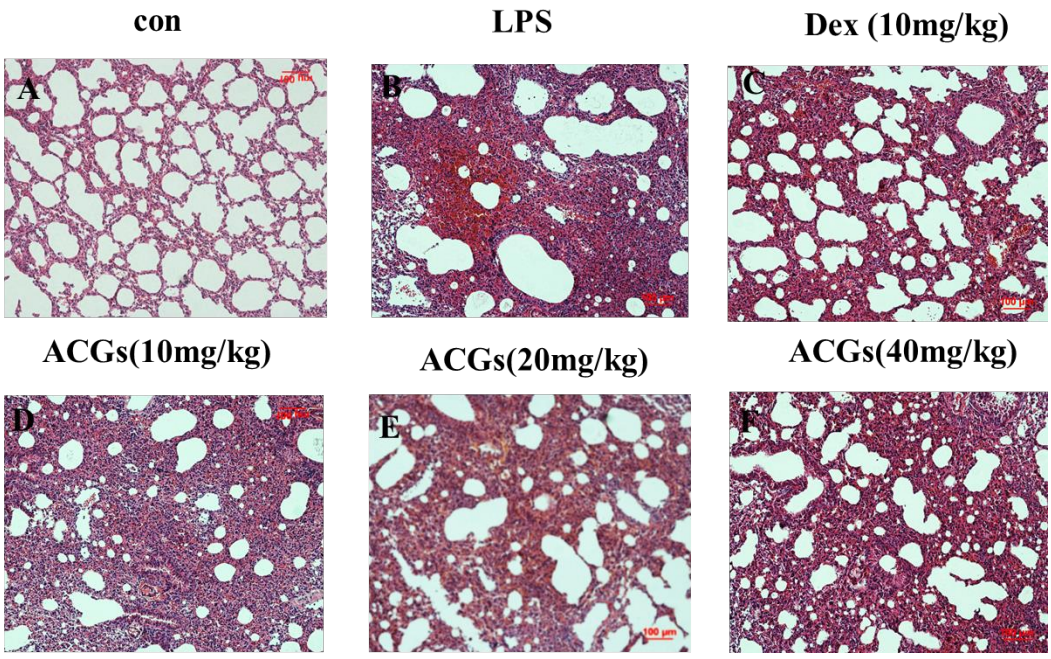

Figure S1. ACGs ameliorated on-going LPS-mediated lung inflammation. (A-F) ACGs were given to the animals 24h after initial LPS treatment (n=6 mice per group). Tissue sections were stained with hematoxylin-eosin to evaluate tissue inflammation.

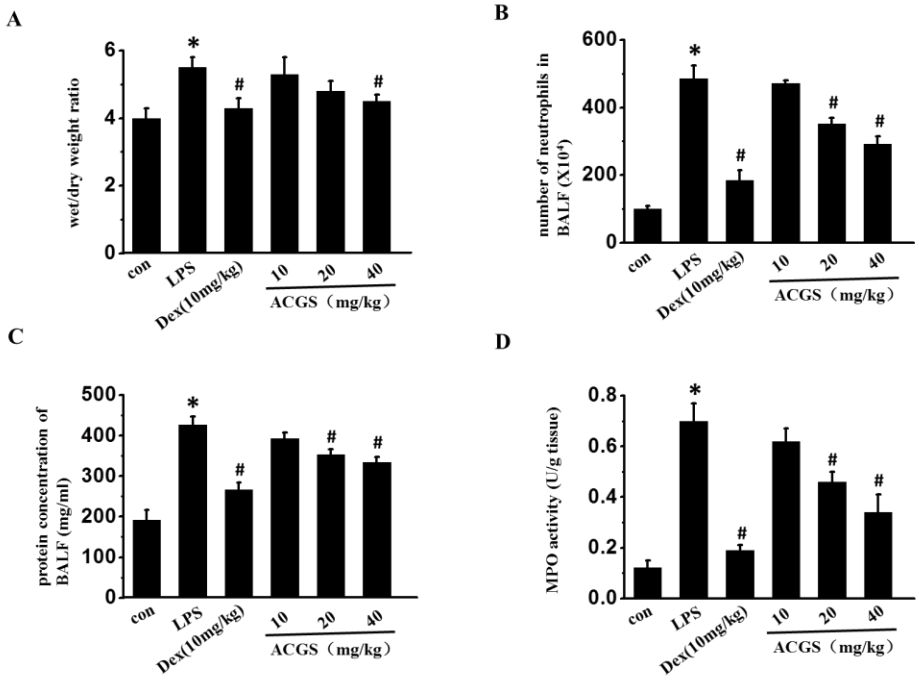

Figure S2. ACGs reduced LPS-induced pulmonary edema and microvascular permeability. (A-D) ACGs treatment was given 24h post LPS treatment, results show wet/dry weight ratio (A), number of neutrophils (B), and amount of total protein in BALF (C) and MPO activity (D) (n=6

mice per group, * P<0.05 vs control (con) group; #P<0.05 vs LPS-treated group).

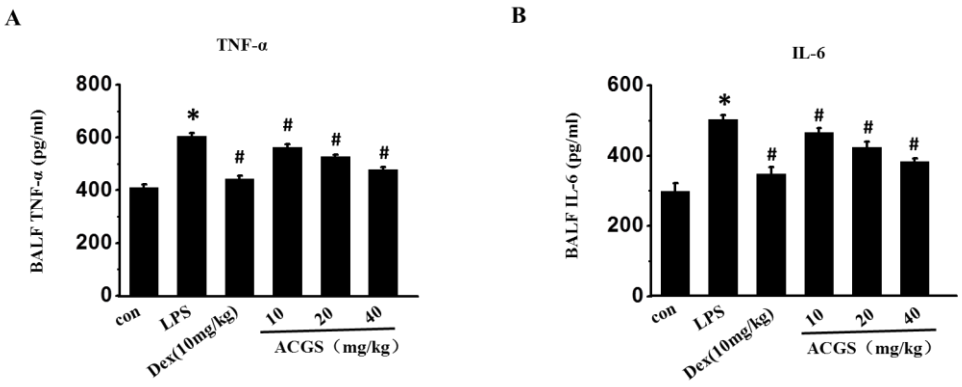

Figure S3. ACGs reduced TNF-α and IL-6 levels in LPS-induced ALI in mice. (A, B) ACGs treatment was given 24h post LPS treatment and TNF-**α** and IL-6 levels were quantified in BALF (n=6 mice per group, * P<0.05 vs con group; #P<0.05 vs LPS treated group).

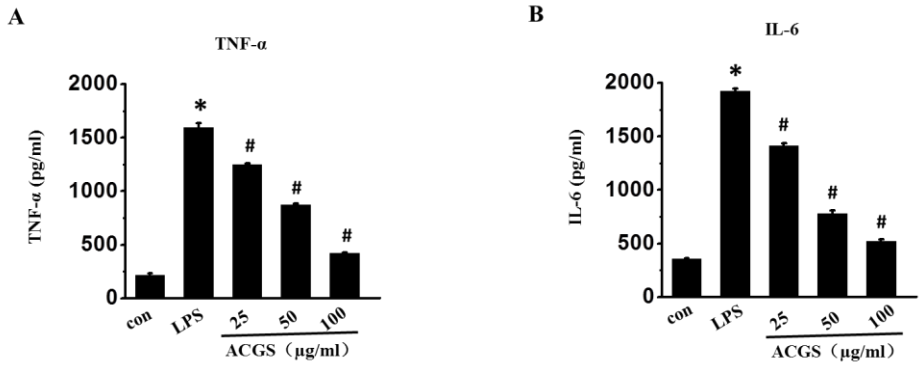

Figure S4. ACGs down-regulate cytokine production by RAW 264.7 cell line in response to LPS. (A, B) RAW 264.7 macrophages were incubated with increasing concentrations (25, 50, 100 μg/ml) of ACGs for 2 h, followed by stimulation with LPS (1μg/ml) for 24 h, when TNF-α and IL-6 concentration was measured by ELISA in cell supernatants. (n=6, * P<0.05 vs control (con) group; #P<0.05 vs LPS treated group).

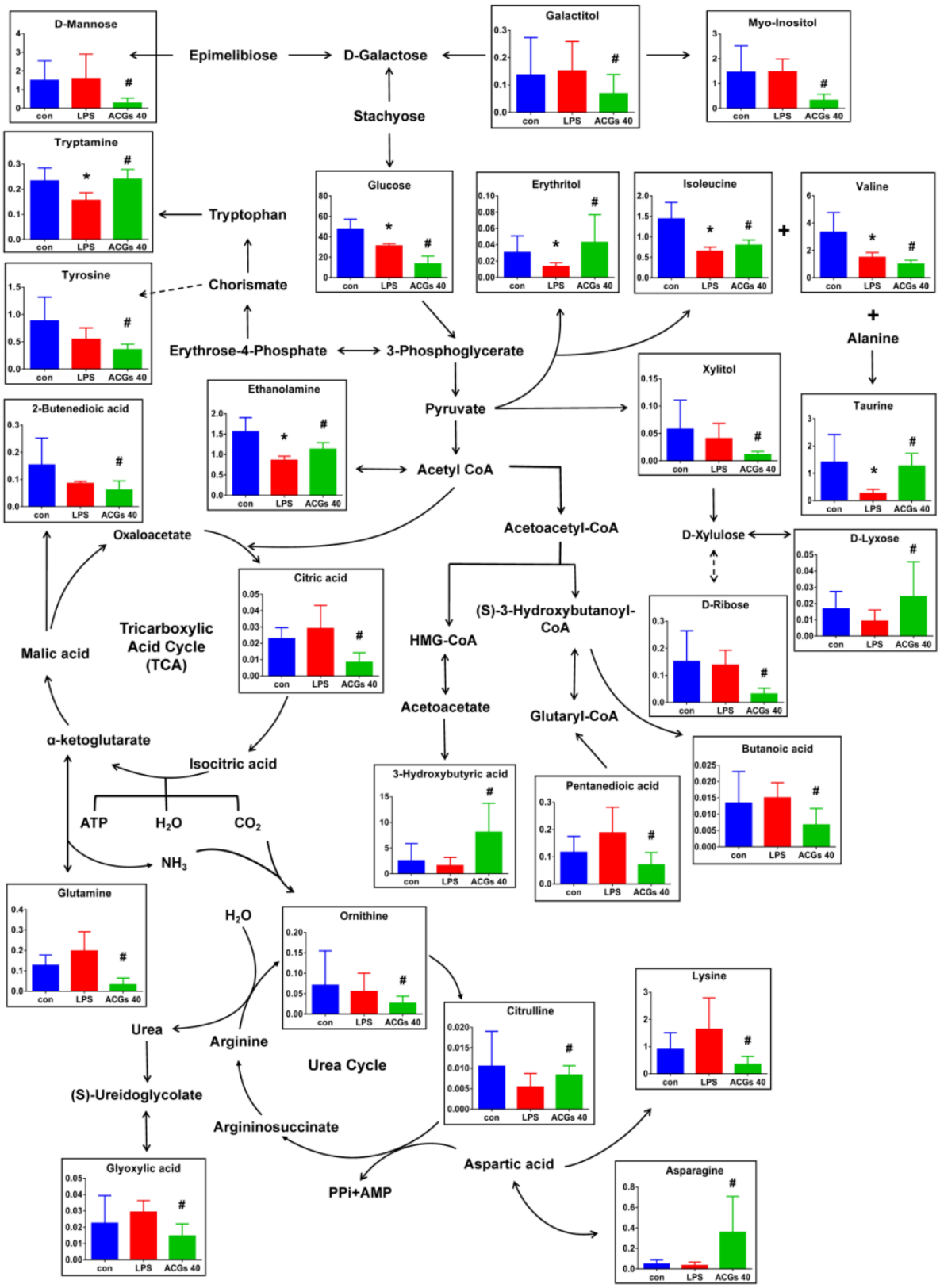

Figure S5. Metabolite network modulated by ACGs during experimental ALI. Metabolites were analyzed in serum of control (con) naïve mice (blue), LPS-treated mice (red) and ACGs/LPS-treated mice (n=6 mice per group, * P<0.05 vs con group; #P<0.05 vs LPS treated group).

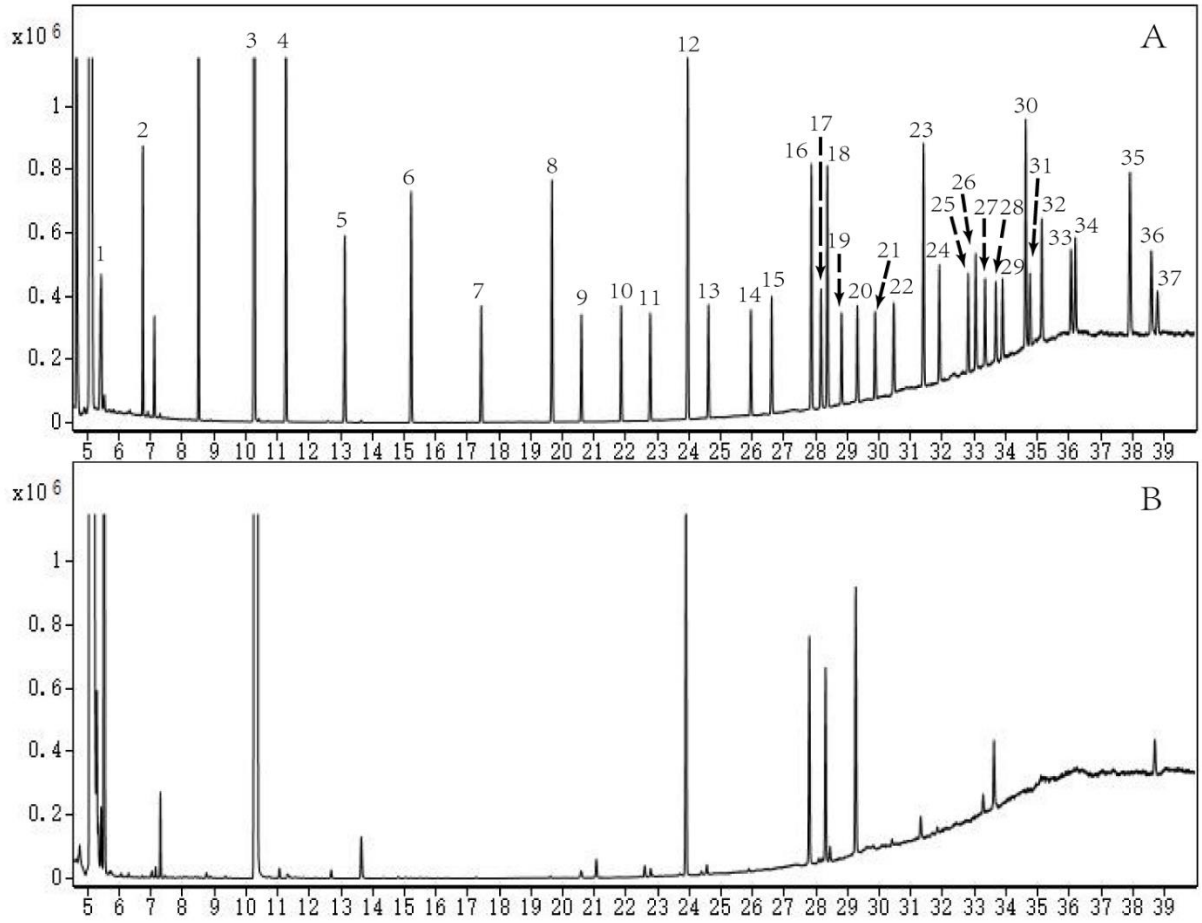

Figure S6-1. Total ion chromatogram (TIC) of targeted profiling of 37 fatty acids. (A) the reference solution of 37 fatty acid methyl esters. **(B)** the lipid extract of serum of control group. **1.** Butanoic acid methyl ester (C4:0); **2.** Caproic acid methyl ester (C6:0); **3.** Caprylic acid methyl ester (C8:0); **4.** Capric acid methyl ester (C10:0); **5.** Undecanoic acid methyl ester (C11:0); **6.** Lauric acid methyl ester (C12:0); **7.** Tridecanoic acid methyl ester (C13:0); **8.** Myristic acid methyl ester (C14:0); **9.** Myristoleic acid methyl ester (C14:1); **10.** Pentadecanoic acid methyl ester (C15:0); **11.** *cis*-10-Pentadecanoic acid methyl ester (C15:1); **12.** Palmitic acid methyl ester (C16:0); **13.** Palmitoleic acid methyl ester (C16:1); **14.** Heptadecanoic acid methyl ester (C17:0); **15.** cis-10-Heptadecenoic acid methyl ester (C17:1); **16.** Stearic acid methyl ester (C18:0); **17.** Stearic acid methyl ester (C18:1n9t); **18.** Oleic acid methyl ester (C18:1n9c); **19.** Linolelaidic acid methyl ester (C18:2n6t); **20.** Linoleic acid methyl ester (C18:2n6c); **21.** γ-Linolenic acid methyl ester (C18:3n6); **22.** Linolenic acid methyl ester (C18:3n3); **23.** Arachidic acid methyl ester (C20:0); **24.** *cis*-11-Eicosenoic acid methyl ester (C20:1); **25.** *cis*-11,14-Eicosadienoic acid methyl ester (C20:2); **26.** Heneicosanoic acid methyl ester (C21:0); **27.** *cis*-8,11,14-Eicosatrienoic acid methyl ester

(C20:3n6); **28.** Methyl *cis*-5,8,11,14-eicosatetraenoic acid methyl ester (C20:4n6); **29.** *cis*-11,14,17-Eicosatrienoic acid methyl ester (C20:3n3); **30.** Behenic acid methyl ester (C22:0); **31.** *cis*-5,8,11,14,17-Eicosapentaenoic acid methyl ester (C20:5n3); **32.** Erucic acid methyl ester (C22:1n9); **33.** *cis*-13,16-Docasadienoic acid methyl ester (C22:2); **34.** Tricosanoic acid methyl ester (C23:0); **35.** Lignoceric acid methyl ester (C24:0); **36.** Nervonic acid methyl ester (C24:1); **37.** *cis*-4,7,10,13,16,19-Docosahexaenoic acid methyl ester (C22:6n3).

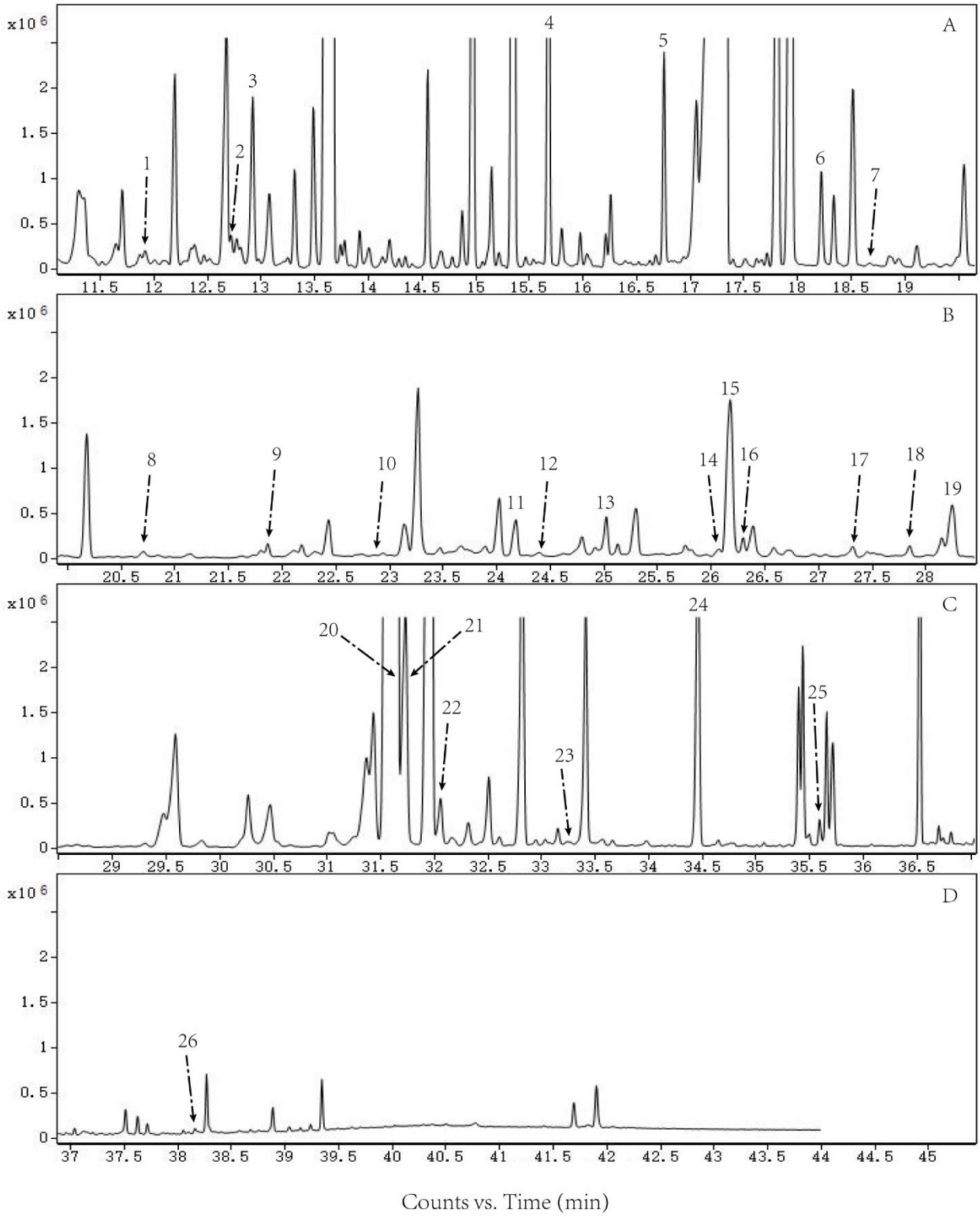

Figure S6-2. Total ion chromatogram (TIC) of non-targeted metabolic profiling of mice serum. **(A)** Acquisition time of 11 ~ 20.5 min. **(B)** Acquisition time of 20.5 ~ 28.5 min. **(C)** Acquisition time of 28.5 ~ 37 min. **(D)** Acquisition time of 37 ~ 45 min. **1.** Glyoxylic acid; **2.** Tryptamine; **3.** Ethanolamine; **4.** 3-Hydroxybutyric acid; **5.** L-Valine; **6.** L-Isoleucine; **7.** Inosose; **8.** Butanoic acid; **9.**

methylmalonic acid; **10.** Citrulline; **11.** Pentanedioic acid; **12.** L-Proline; **13.** D-Ribose; **14.** Asparagine; **15.** Taurine; **16.** Arabinofuranose; **17.** Xylitol; **18.** DL-Ornithine; **19.** L-Glutamine; **20.** d-Glucose; **21.** L-Lysine; **22.** L-Tyrosine; **23.** meso-Erythritol; **24.** Myo-Inositol; **25.** L-Tryptophan; **26.** Doconexent.

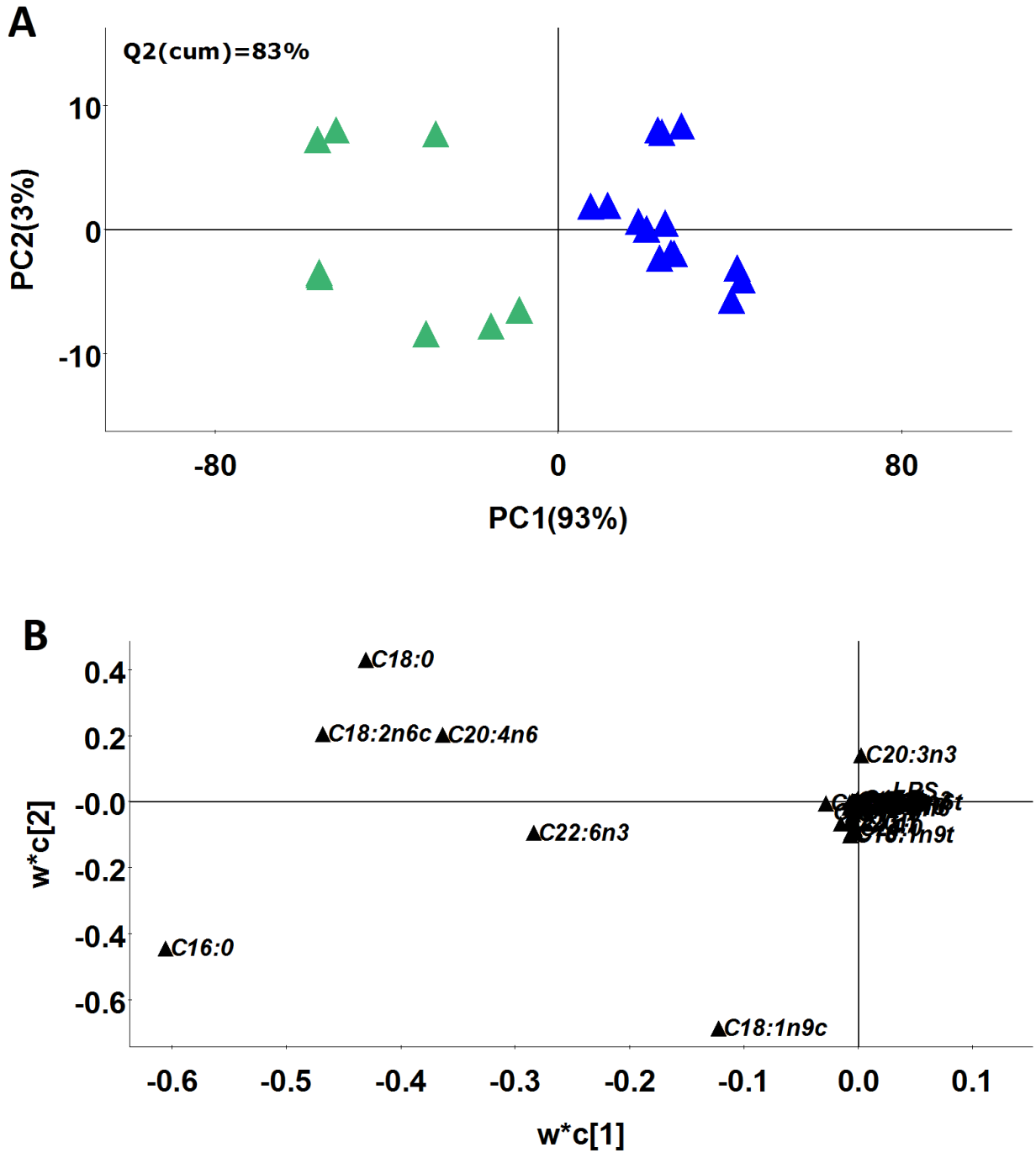
A
Q2(cum)=83%
10
0
-10
PC2(3%)
-80
0
80
PC1(93%)
B
0.4
0.2
-0.0
-0.2
-0.4
-0.6
w*c[2]
C18:0
C18:2n6c
C20:4n6
C20:3n3
C22:6n3
C16:0
C18:1n9c
-0.6
-0.5
-0.4
-0.3
-0.2
-0.1
0.0
0.1
w*c[1]

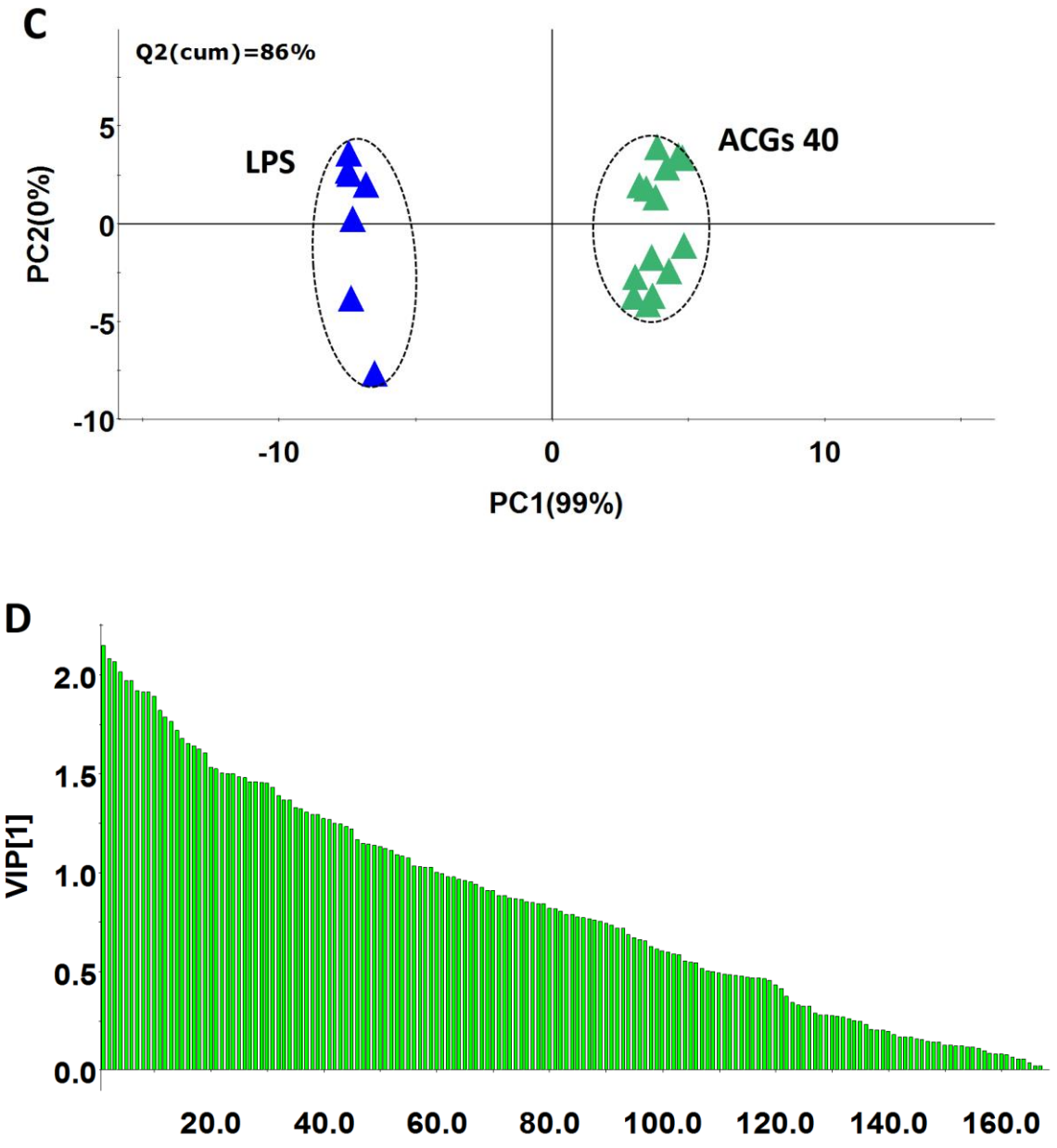

Figure S7. The pattern recognition analysis of differential metabolites in ACGs group versus LPS group. (A) The scores plot of PLS-DA for fatty acids in LPS group and ACGs group (40 mg/kg) [$R^2Y(cum)$ = 0.8766, $Q^2(cum)$ = 0.8290]. **(B)** Loading of PLS-DA for fatty acids in LPS group and ACGs group (40 mg/kg). **(C)** The scores of OPLS-DA for water-soluble metabolites in LPS group and ACGs group (40 mg/kg) [$R^2Y(cum)$ = 0.9890, $Q^2(cum)$ = 0.8559]. **(D)** VIP of OPLS-DA for water-soluble metabolites in LPS group and ACGs group (40 mg/kg). **"LPS",** LPS group; **"ACGs 40",** apigenin C-glycosides group (40 mg/kg). LPS group was presented by blue triangles and ACGs group (40 mg/kg) was the triangles of green.

Supplemental Table S1 Physical function analysis using IPA generated the molecular interaction networks which are ordered by a score denoting significance. The highest-scoring network, which comprises 16 molecules in our list, revealed significant changes in "Cellular compromise, Lipid metabolism, Small molecule biochemistry". A marked molecular networks with inflammatory regulators like pro-inflammatory cytokines, c-Jun N-terminal kinase (JNK), extracellular regulating kinase 1/2 (ERK 1/2), caspase-3/7 and so on, was clearly presented.

ID	Molecules in Network	Score	Focus Molecules	Top Diseases and Functions
1	**(R)-3-hydroxybutyric acid**, ADCY, Alp, AMPK, **arachidonic acid**, arginase, Caspase 3/7, **citrulline**, Collagen type IV, CPT1, cytochrome C, **D-glucose**, ERK 1/2, **ethanolamine**, **glutaric acid**, Growth hormone, hexokinase, IL-1, JINK 1/2, **L-glutamine**, **L-lysine**, **L-proline**, **L-tryptophan**, LDL, **linoleic acid**, **methylmalonic acid**, NADPH oxidase, Nr1h, **palmitic acid**, Pro-inflammatory Cytokine, Proinsulin, Sod, **stearic acid**, **taurine**, **xylitol**	43	16	Cellular Compromise, Lipid Metabolism, Small Molecule Biochemistry
2	26s Proteasome, advanced glycation end-products, Akt, ANGPT4, **butyric acid**, Cyp2j9, ERK, Fetal Hemoglobin, Focal adhesion kinase, GRIN3A, GsK3, H2BFM, lgf, Insulin, Jnk, KSR2, **L-tyrosine**, Mapk, NFκB (complex), nicotinamide adenine dinucleotide phosphate, NMDA Receptor, P38 MAPK, PI3K (complex), Pkc(s), PKDCC, PKHD1, PP2A, PTPN7, Ras, **ribose**, RNF141, **taurine**, tyramine, Vegf, VTCN1	8	4	Cellular Compromise, Cell Cycle, Embryonic Development